SkillWeave: Evidence-Driven Co-Evolution of Instructions, Code, and Workflows for Scientific PDF Translation

CHENG ZENG

zengcheng4747@gmail.com

Abstract

Agent skills in production systems are jointly determined by natural-language instructions, executable code, persistent workflow state, and verification logic. Scientific PDF translation exposes the interaction among these components particularly clearly: a fluent target paragraph can coexist with omitted source prose, damaged mathematical notation, incorrect object ownership, or a misleading completion status. We introduce SkillWeave, a framework for turning such failures into evidence-driven updates at the appropriate system layer. The framework traces each observed defect through source extraction, translation catalogs, accepted text, layout composition, and rendered artifacts; it then records whether the resulting change belongs in instructions, code, workflow control, verification, or a document-local repair.

We evaluate the framework through four engine versions, six fixed fixtures, 48 mechanism probes, seven full or ablated conditions, and eight native-region restoration trials. Across the four normal fixtures, shared acceptance rose from 3/4 to 4/4. Recognition of 24 mathematical positives rose from 0/24 to 24/24 while 24 negative probes retained zero false positives. Removing either of two recognition mechanisms lost 12 positives, and all eight restoration trials satisfied both source-region fidelity and outside-region consistency checks. A subsequent longitudinal case study on three pages of a real paper shows how deterministic layout invariants, inherited SVG clipping, glyph ownership, and source-coverage checks emerged from repeated use. These results establish evidence for specific engine mechanisms and motivate a document-level protocol for evaluating instruction effects, transfer, and semantic quality.

1. Introduction

A visible failure in a translated paper rarely identifies its own cause. A missing superscript may originate in the language model, the extractor, the layout engine, or the verifier. Likewise, a job may report that every issued translation entry has been submitted while source prose remains absent from the catalog. The engineering problem is therefore broader than prompt revision: the system must determine which component failed, preserve enough evidence to support that diagnosis, and place the correction where future tasks can reuse it.

Prior work provides several useful pieces of this process. SkillOpt proposes budgeted edits to skill text under a fixed execution harness and selects candidates using task traces (Yang et al., 2026). GEPA studies reflective prompt evolution (Agrawal et al., 2025), while TextGrad treats textual feedback as a mechanism for optimizing compound AI systems (Yuksekgonul et al., 2024). SkillsBench evaluates skills through matched task conditions (Li et al., 2026), and EvoSkill and SkillFoundry address the discovery and evolution of reusable skill libraries (Alzubi et al., 2026; Shen et al., 2026). Building on these ideas, SkillWeave studies a different but complementary question: when a real document fails, should the experience update instructions, executable mechanisms, workflow state transitions, verification, or a bounded repair artifact?

Scientific PDF translation makes this question concrete because the output combines language, geometry, and native document objects. The relevant quality dimensions include semantic fidelity, source coverage, formula preservation, navigation, readable layout, and an honest delivery state. A single scalar "success" label obscures the mechanisms that produce those dimensions. We therefore represent system evolution as a set of layer-specific changes supported by explicit artifacts and reproducible checks.

The translation pipeline uses the host language model for terminology selection and target-text generation, supported by deterministic source analysis and PDF composition. Visual feedback then informs local repairs and reusable engine updates. This division of work supports both source-aware translation and efficient revision: compatible unchanged pages can be reused while corrected pages are regenerated and inspected.

Our contributions are fourfold:

- We formulate skill evolution as coordinated updates to instructions, code, workflow, and verification, with evidence routing that links visible failures to these layers.
- We provide controlled version replay, mechanism probes, and targeted ablations that isolate two mathematical-object recognition mechanisms.
- We distinguish catalog completion, source coverage, visible target coverage, native-object fidelity, and semantic review, and show why each requires separate evidence.
- We report document cases connecting local defects to reusable coverage, caption, clipping, and glyph-ownership rules, together with a measured page-reuse experiment and a protocol for model-level attribution.

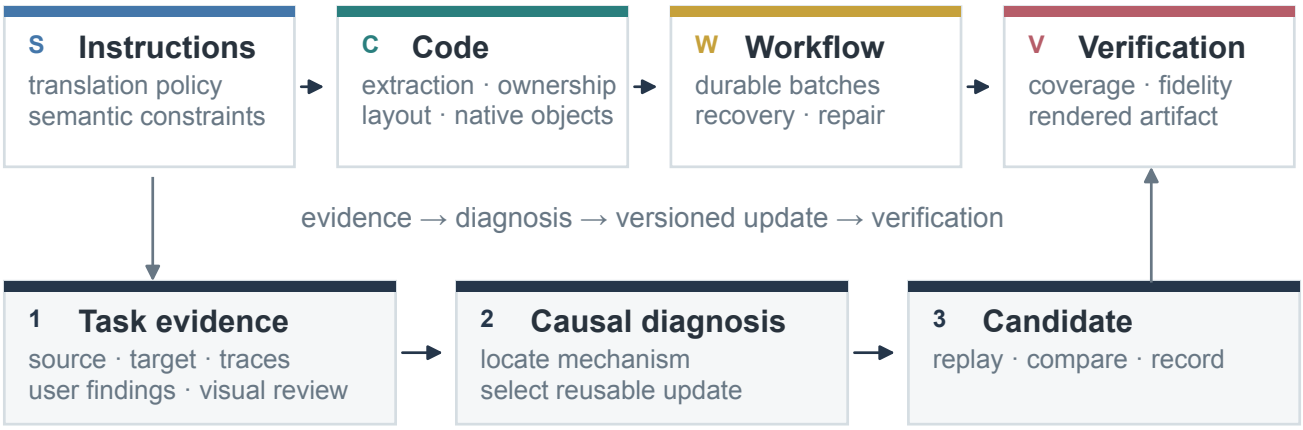


Figure 1. The SkillWeave evidence loop. The upper row contains four independently evolvable components. The lower row turns task artifacts into a causal diagnosis and a versioned candidate that is replayed under verification.

Table 1. Positioning of SkillWeave relative to related work. The final column identifies the connection rather than a performance ranking.

Work	Primary object of study	Connection to SkillWeave
SkillOpt (Yang et al., 2026)	Skill text, task traces, and candidate selection	Motivates controlled edits and validation-separated selection
GEPA (Agrawal et al., 2025)	Reflective prompt evolution	Motivates experience-driven candidate generation
TextGrad (Yuksekgonul et al., 2024)	Textual optimization in compound AI systems	Establishes prior work on multi-component textual feedback
SkillsBench (Li et al., 2026)	Paired evaluation of skill utility across tasks	Motivates matched execution conditions
EvoSkill / SkillFoundry (Alzubi et al., 2026; Shen et al., 2026)	Discovery and evolution of reusable skill libraries	Relates to experience accumulation and reusable mechanisms
SkillWeave	Instructions, engines, workflows, verification, and rendered artifacts	Focuses on scientific-object fidelity and evidence scope

2. Problem Formulation and Causal Diagnosis

Let d denote a source PDF and M the host model. We represent the system state as

$$Z = (S, C, W, V), \tag{1}$$

where S contains instructions and translation policies, C contains executable extraction and layout mechanisms, W contains persistent workflow state and recovery logic, and V contains mechanical and visual verification. Executing the system produces a candidate artifact y and trace τ; verification produces evidence e:

$$\begin{aligned}(y, \tau) &= H(M, d; S, C, W),\\ e &= V(d, y, \tau).\end{aligned} \tag{2}$$

An update is a structured change $\Delta Z = (\Delta S, \Delta C, \Delta W, \Delta V)$. A single defect may require more than one component. For example, repairing a damaged formula may require both native-object restoration in C and a new preservation check in V.

2.1 Executable Boundaries Determine Repair Scope

A translation client can fill only entries that the extractor has issued. Source prose outside the catalog therefore requires either an extraction update or a post-processing path that reads the source region directly. This interface boundary distinguishes mechanical composition from host-assisted document repair. It also explains why complete submission of issued entries cannot establish complete source coverage.

2.2 Reusable Rules and Document Repairs

A reusable update is expressed through conditions such as font identity, glyph geometry, syntax, column membership, or local spatial relations, and it is replayed on additional samples. A document-local repair may use coordinates specific to one PDF, so its evidence applies to that artifact. The repair becomes a claim about general capability only after its mechanism has been abstracted into document-independent conditions and tested beyond the original page.

3. Method: Evidence-Driven Multi-Layer Updates

3.1 End-to-End Translation Workflow

The automated translation pipeline combines a vision-capable language model with a deterministic Python document engine.

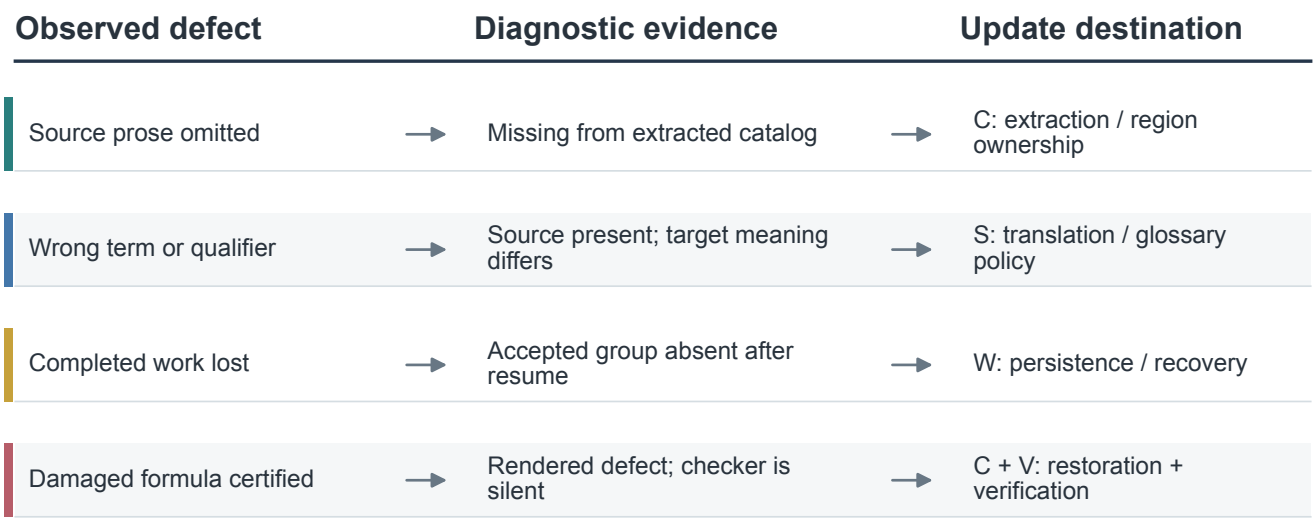


Figure 2. Examples of evidence routing. Each visible defect is linked to the intermediate evidence needed for diagnosis and to the system component that owns the reusable correction.

The model generates translations within this pipeline, while Python manages extraction, document structure, composition, and validation. We use *mechanical layout* specifically for the programmatic operations that consume accepted target text and produce a PDF. A complete translation task follows six stages:

1. **Create and extract.** The engine records the source PDF, selected pages, language pair, and policies in a durable job. It extracts text regions and page geometry, identifies protected scientific objects, and creates a translation catalog with stable identifiers and mathematical placeholders. An independent source-block audit identifies potential omissions for inspection.
2. **Prepare context and translate.** Python gathers terminology candidates and geometric evidence for words split across lines or columns. The host model reviews this evidence in the paper's context, establishes a shared glossary, and generates target-language text while preserving mathematical and link placeholders. Short extracts use one worker; longer documents may distribute consecutive groups across workers. Completed batches are collected promptly so that subsequent groups can proceed.
3. **Collect and compose.** Python validates response structure, saves available translations, and composes the bilingual PDF. It controls fonts, line wrapping, source anchors, glyph ownership, clipping, and native-object restoration. Programmatic checks produce a separate issue checklist alongside the candidate.
4. **Inspect visually.** The host renders the actual candidate and compares every requested page with the source at readable resolution. This review checks source coverage, legibility, formulas, figures, captions, and visible overlap or clipping. An additional independent linguistic review can be requested separately.
5. **Repair and recheck.** The model diagnoses visible defects and selects an existing local repair or authors a bounded correction. Python recomposes changed pages and reassembles the complete PDF, reusing compatible unchanged pages. The model inspects newly rendered or repaired pages; prior visual review is retained for verified unchanged pages.
6. **Deliver and retain evidence.** The host delivers the final PDF and its issue checklist, preserving the job, accepted text, intermediate candidates, and repair records for recovery and subsequent skill improvement. An unresolved content or layout defect remains explicit in the delivery status.

Candidate availability is a prerequisite for visual verification. The engine therefore materializes available target text before applying acceptance criteria. When ordinary composition fails, source-anchored recovery or a page-local emergency renderer retains the translated content for inspection. Output availability, programmatic checks, visual verification, and final acceptance are tracked separately. Diagnostics are stored with the candidate in an issue checklist and repair manifest, leaving the document's reading area available for its original content.

3.2 Inference Cost and Host-Model Requirements

The automated translation pipeline incurs model usage during terminology selection and translation generation, followed by visual inspection, semantic judgment, and any required repair reasoning or code generation. Its deterministic Python components—extraction, validation, composition, rasterization, and execution of saved repairs—consume compute time and memory without model inference. Zero-token execution therefore applies to these programmatic components. Orchestration adds token usage when the host reads instructions, context, images, or tool results and decides subsequent actions. We account for the model-assisted pipeline and its mechanical-layout component separately.

Token accounting distinguishes context preparation and translation, review, repair reasoning, and orchestration, with each component including its applicable input and output usage. Vi-

sual review additionally incurs image-input usage according to the host model's accounting scheme. Mechanical-layout runtime is recorded separately. Reusing accepted translations avoids regeneration, while consolidating diagnosis and repairs reduces repeated model interactions. The runtime measurements in Section 5.4 describe elapsed execution; token usage requires separate instrumentation.

The end-to-end host requires visual input capability together with scientific-language competence, instruction following, and tool use. It must be able to compare rendered pages with the source and inspect small mathematical or graphical details. Text-only workers may generate translation groups when a vision-capable host performs the page review and repair loop. Model quality can affect terminology, semantic fidelity, defect detection, and the quality of repair decisions. Deterministic layout rules and native-object preservation are designed to constrain variation in document geometry across capable host models. We therefore expect broadly comparable layout quality among models that satisfy these requirements, while the magnitude of remaining differences in language quality and repair success calls for a controlled cross-model evaluation.

3.3 Source-Aware Translation and Composition

Document-wide terminology preparation links language generation to source structure. Python proposes recurring technical terms, model and dataset names, and abbreviation definitions from the requested catalog. The host model selects their translations using representative context and supplies the resulting glossary to every translation group. Geometry-backed reading hints identify hyphenated words and adjacent column fragments while preserving the original source entries. The model resolves ambiguous joins and terms in context, and the durable job retains a stable glossary across batches.

Source coverage is checked independently of catalog submission. The audit reads source text blocks and compares their spatial and textual support with translated regions, flagging prose, titles, captions, and notes that may have been omitted or absorbed into preserved objects. Findings retain their page and region identity, including repeated text at different locations. The host distinguishes genuine omissions from intentionally preserved table cells, chart interiors, author information, code, and references. Available translations remain renderable while these findings are investigated.

Composition assigns ownership at a finer granularity than a whole table or figure envelope. Table titles and captions enter the translation catalog while cells and numerical data retain their native appearance. Geometrically connected caption lines are merged across font-weight changes, with independent headings preserved as separate regions. Plot labels and digits remain attached to their graphics; prose and footnotes retain their own mathematical objects. Native bullet evidence preserves list boundaries, and numbered URL footnotes retain their source alignment. Recognizable marginal stamps are removed from the target side when their bounds are clear of prose, while the source panel preserves the original page.

Local prose repairs use the same registered fonts, measured layout, and native formula assets as ordinary composition. This shared repair interface checks font roles, glyph availability, spacing, and region bounds before producing a candidate for visual inspection. It makes the typography and mathematical-preservation rules reusable across routine composition and host-directed repairs.

3.4 Failure Records

Each failure record identifies the source page, output page, region, observed damage, expected behavior, and evidence path. Diagnosis proceeds through the source PDF, extracted page model, translation catalog, accepted target text, layout manifest, and final render. This sequence distinguishes three materially different states: source content omitted during extraction, accepted content omitted during rendering, and content rendered with an incorrect meaning or appearance. Durable records also allow a later session to resume from the same evidence rather than reconstructing the failure from memory.

3.5 Stable Update Locations

Open-source implementation reference. The formula-preservation implementation draws on the open-source BabelDOC codebase (BabelDOC contributors, 2026), particularly its treatment of formula characters as structured intermediate objects. This design informed the handling of glyphs with unreliable Unicode mappings: the engine identifies native glyphs through their geometric envelope and baseline alignment, then preserves their source appearance during bilingual composition. The corresponding implementation records this connection in its formula-object module.

Conventions requiring semantic judgment belong in S, including terminology, qualifications, and preservation of complete meaning. Deterministic constraints belong in C, including column boundaries, glyph ownership, source-native formula restoration, and marker order. Interruption recovery, partial submission, and retries belong in W. Independent source coverage, native-object comparison, and final-artifact inspection belong in V. Recording the selected layer keeps the natural-language skill description aligned with the actual engine behavior.

3.6 Incremental Page Revision

Revision reuses verified mechanical artifacts at page granularity. The engine computes a signature from each page's frozen model and accepted translation entries, then compares it with the latest compatible completed attempt. Reuse also depends on source identity, engine fingerprint, fonts, render policy, and artifact hashes. Changed pages are rendered and substituted into the complete PDF; unchanged page diagnostics are retained, and global page mapping and navigation are checked again. An incompatible or damaged cache triggers the appropriate full processing path.

The cache is bound to an immutable mechanical attempt. Separately saved host repairs are tracked in their own manifest and reapplied where needed after revision. Visual review follows the resulting changes: newly rendered and repaired pages are inspected, while verified unchanged pages retain their earlier review. This design limits local revision work while preserving the provenance of both programmatic and host-directed modifications.

Table 2. Reusable update units abstracted from observed failures.

Failure mechanism	Reusable update	Verification target
Oversized mathematical font cell shields prose	Share concrete glyph identity between prose removal and formula restoration	Adjacent prose and mathematical ink
Cross-column formula grouping	Enforce column membership during formula composition	Independent objects on the same baseline
Local overflow degrades a full document	Preserve only affected pages while healthy pages continue composition	Affected-page set and document status
Catalog completes while title or caption is absent	Verify titles, captions, and appendices against source regions	Source coverage outside catalog counts
Recovery reissues completed groups	Collect saved responses before dispatching remaining work	Accepted groups and submission history

3.7 Bounded Changes and Persistent Evidence

We record modification budgets as a vector containing edited instruction paragraphs, code modules, and workflow transitions. These components have different meanings and should not be collapsed into a single learning-rate metaphor. Every candidate is linked to an engine version, source input, replay command, artifact hashes, and an acceptance decision. The current implementation includes durable translation jobs, public submission and revision interfaces, a model-assisted translation pipeline, and bounded native-region repair. Automated routing and long-horizon candidate scheduling remain targets for future system work.

Repair prioritizes missing content and visible damage to text, formulas, tables, or figures. Triage excludes fully off-page drawing objects and groups repeated findings by page, object, and cause. The host consolidates diagnosed defects into one repair candidate and reinspects the affected regions; an additional pass addresses a concrete residual defect. Configurable time checkpoints limit extended diagnosis and route reproducible mechanism failures to engine maintenance. Diagnosis, repair authoring, execution, rendering, and review are recorded separately so that model interaction cost can be distinguished from program runtime.

3.8 Candidate Acceptance

System evolution balances quality and cost. We represent an outcome by

$$Q = (q_{\text{sem}}, q_{\text{src}}, q_{\text{obj}}, q_{\text{nav}}, q_{\text{layout}}, -c), \tag{3}$$

where the components measure semantic fidelity, source coverage, object fidelity, navigation, layout, and cost. Missing observations remain explicitly unscored. Hard requirements such as complete critical prose and intact formulas are evaluated before speed. A candidate is accepted when all hard constraints hold, a declared primary metric improves, and no protected metric regresses.

Verification itself evolves and therefore requires external anchors. A reduced warning count can indicate either a repaired generator or a relaxed checker. We distinguish these explanations with previously fixed translations, independently authored source expectations, expected formula-object counts, and rendered comparisons. Product-policy changes, such as preserving an unsafe page with an explicit incomplete status, are evaluated separately from normal translation quality.

4. Experimental Setup

The controlled study was executed on one macOS host with Python 3.11.9 and a fixed dependency environment. Three historical engines were unpacked from their recorded wheels, while version 0.4.1 was copied from a source snapshot. Each version ran under an isolated working directory and `PYTHONPATH`; module paths, package hashes, and full commands are preserved with the evidence.

The page-reuse experiment separately measures one local revision to a six-page CLIP extract using saved target text. Supporting regressions exercise extraction, source coverage, context preparation, repair typography, and cache validity on the revised implementation. These records have their own source and runtime fingerprints, preserving the configuration of the historical cross-version experiments.

4.1 Fixed Fixtures

Four normal fixtures cover a single-column page, a two-column page, formulas and links, and a page containing a table, figure, and footnote. Two stress fixtures cover an expanded translation that exceeds local capacity and a scan without a text layer. Source expectations and target references were authored independently of current extraction. The expansion case measures capacity handling, while the scan case exercises the OCR boundary and delivery status.

4.2 Mechanism Probes

The probe set crosses two fonts (Times Italic and Helvetica Oblique), three sizes (10, 12, and 15 pt), two page-position configurations, and four content roles. Inline variables and standalone equations form 24 positives; italic emphasis and the pronoun “I” form 24 negatives. These probes intentionally target known mechanism families. Their role is to expose causal behavior under controlled variation; document-level generalization is evaluated separately.

4.3 Ablation and Scoring

Each ablation runs in an isolated process that temporarily disables recognition of short italic algebra, context-sensitive italic variables, or both. Positive probes pass when the expected native mathematical object is detected; negatives pass when no object is created. Cross-version fixtures use shared source, target, object,

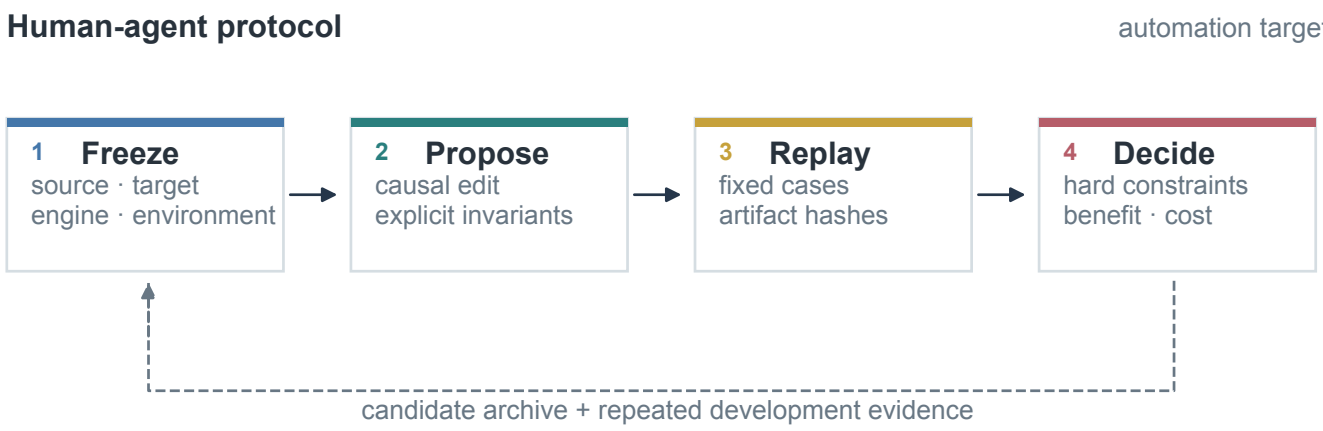


Figure 3. Candidate-gating protocol. Inputs and environments are frozen before a causal change is proposed. Repeated development replay remains attached to the candidate history, while final evaluation uses document-level separation.

Table 3. Experimental scale and the question addressed by each component. Conditions share templates and therefore are reported separately from independent document counts.

Experiment	Scale and controls	Question
Cross-version replay	4 versions × 6 fixed fixtures = 24 tasks	How did engine and delivery behavior change?
Structural probes	48 PDFs × 7 conditions = 336 extractions	How do known mechanisms respond to font and geometry variation?
Mechanism ablation	Full, no algebra, no context, and neither	Which recognition mechanism explains the gain?
Native restoration	8 damage injections, 2 pages checked per case	Does local restoration preserve the target and its surroundings?
Regression suite	540-test study run and 572-test later run	Do the measured changes preserve existing behavior?

and layout requirements. Stress fixtures are evaluated through their delivery state and page-preservation behavior.

5. Results

5.1 Cross-Version Replay

Single-column, two-column, and table/figure fixtures pass in all four versions. The formula fixture changes when ordinary-font mathematical recognition is introduced. Because a version comparison reflects the entire codebase, this result establishes a system-level difference. The ablation study below then narrows the explanation to two recognition paths.

The change in the stress cases concerns failure isolation and status semantics. Version 0.4.x preserves the affected source page and records `translation_complete=false`; healthy pages remain composable, and accepted translations remain recoverable. We report this contract separately from normal translation quality.

5.2 Mechanism Probes and Ablation

Disabling short-algebra recognition removes protection from every standalone equation while leaving context-supported inline variables intact. Disabling context recognition produces the complementary pattern. Removing both reproduces the recognition behavior of versions 0.2.0 and 0.3.1. The 24 negatives retain zero false positives across all conditions, showing that the tested emphasis and pronoun structures remain separated from mathematical objects. A broader independent corpus is needed to estimate precision in naturally occurring papers.

5.3 Catalog Completion and Visible Delivery

Catalog coverage asks whether issued entries were submitted. Source coverage determines whether the catalog denominator includes the required source prose. Rendered coverage then asks whether accepted text appears on the target panel. Occlusion, vector-formula damage, and semantic errors require rendered and semantic review. Treating these measurements separately prevents a completed catalog from standing in for a completed document.

5.4 Runtime Cost

The cost of a delivered artifact is better described as a sum of stages:

$$T_{\text{delivery}} = T_{\text{extract}} + T_{\text{translate}} + T_{\text{layout}} + T_{\text{repair}} + T_{\text{verify}}. \tag{4}$$

The controlled replay measures only part of this expression. In an earlier scheduling observation, 17 entries containing 6,612 source-template characters took 229.42 seconds with serial model calls and 109.77 seconds with three-way parallelism, a 52.15% reduction for that task. We retain this observation as evidence about scheduling, while stable acceleration requires repeated measurements under a common delivery contract.

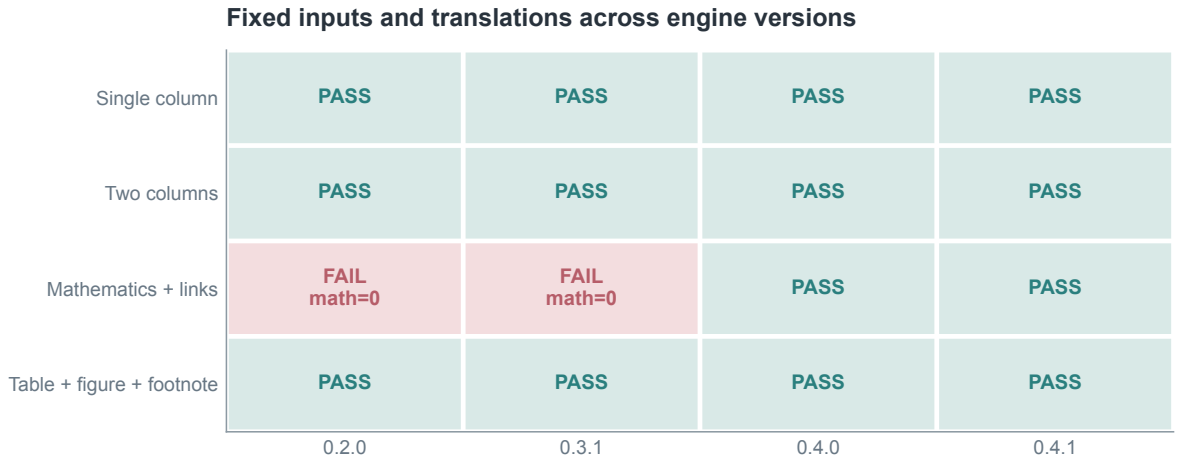


Figure 4. Replay of four normal fixtures with identical source files and fixed translations. Earlier versions satisfy text coverage on the mathematics fixture but create no native formula objects; versions 0.4.0 and 0.4.1 recognize the protected objects and pass the shared acceptance conditions.

Table 4. Normal fixtures and stress behavior. Scanned pages follow the explicit `needs-ocr` path.

Version	Normal fixtures passed	Formula objects	Expansion stress	Scan
0.2.0	3/4	0	Draft with findings	`needs-ocr`
0.3.1	3/4	0	Draft with findings	`needs-ocr`
0.4.0	4/4	2	Page preserved; complete=false	Page preserved; `needs-ocr`
0.4.1	4/4	2	Page preserved; complete=false	Page preserved; `needs-ocr`

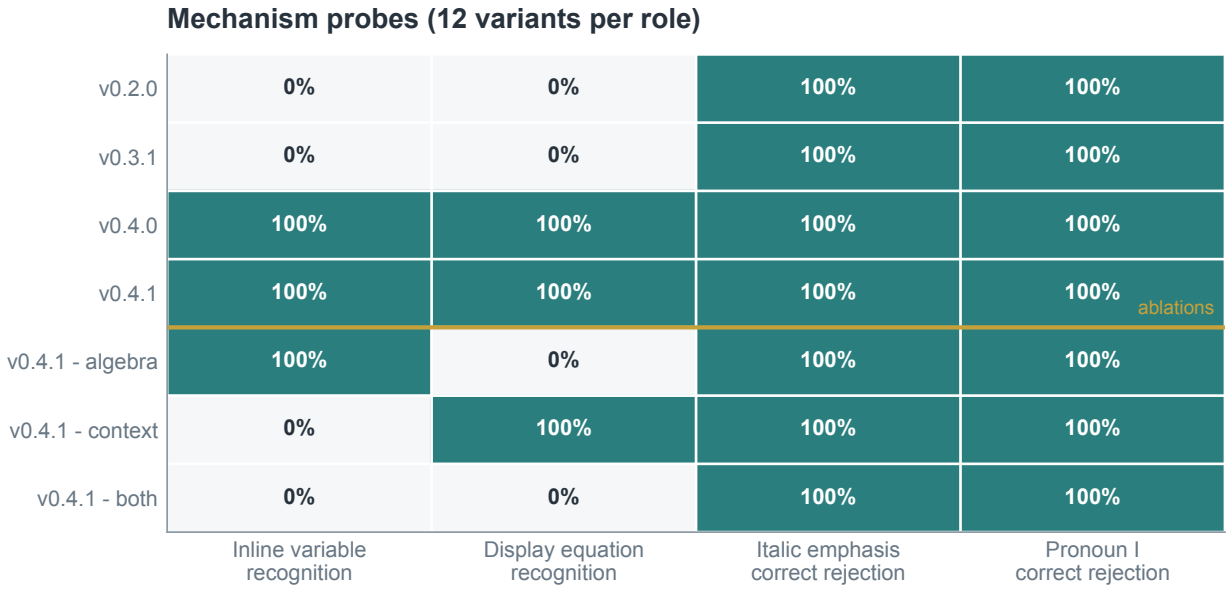


Figure 5. Probe results. Each cell aggregates 12 structural variants. The upper rows compare versions; the lower rows remove recognition mechanisms from version 0.4.1.

Incremental revision cost. A recorded CLIP experiment used six nonconsecutive source pages (4, 10, 21, 22, 44, and 46) and 73 previously accepted translation entries matched by exact source template and paragraph count. Following full generation, one meaning-preserving text revision on page 10 triggered incremental processing. Table 7 reports 65.75 versus 9.65 seconds for composition and 93.74 versus 37.11 seconds for the complete finalization call, corresponding to speedups of 6.81 and 2.53, respectively. The other five pages had identical rendered pixels at the same resolution, and their existing diagnostics were retained. Preflight still took 23.03 seconds for the revised complex page and global checks. These measurements characterize one layout-and-validation revision with saved translations; language generation and host review have separate costs.

Table 5. Ablation in version 0.4.1.

Condition	Pass	TP	FP	Precision / Recall
Full	48/48	24	0	1.00 / 1.00
No short algebra	36/48	12	0	1.00 / 0.50
No context rule	36/48	12	0	1.00 / 0.50
Neither	24/48	0	0	– / 0.00

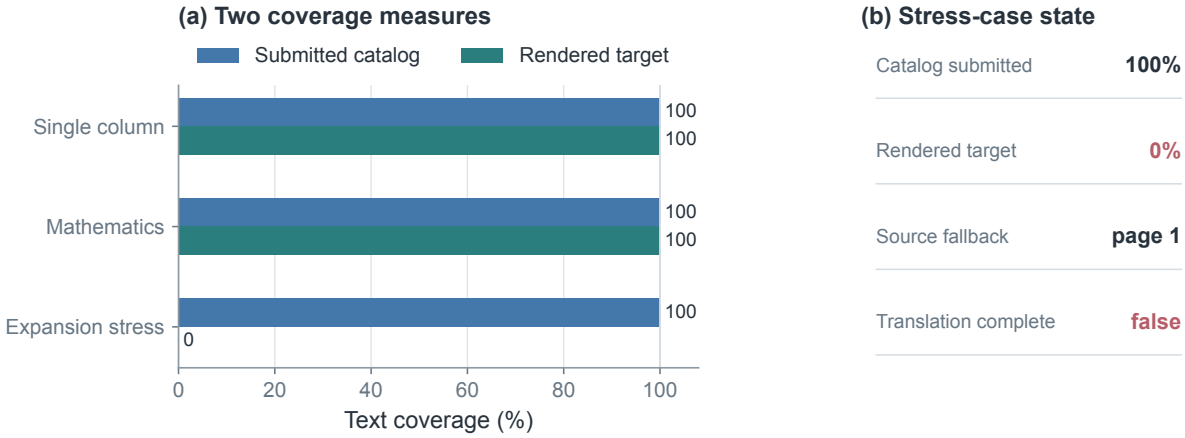


Figure 6. Catalog submission and rendered target coverage answer different questions. In the expansion stress case, every issued entry is submitted while the target panel contains none of the expected translation and the task explicitly records an incomplete delivery.

Table 6. Quality measurements and the evidence that complements each one.

Measurement	Directly supported judgment	Complementary evidence
Catalog coverage	Submission of issued entries	Source coverage for catalog omissions
Source-fragment coverage	Inclusion of annotated source fragments	Broader annotation for document completeness
Target text-layer coverage	Extractability of expected target text	Rendering and semantic review for occlusion and meaning
Mechanical certification	Passage of implemented checks	External rendering and source comparison for blind spots
Rendered or semantic review	Visual or semantic quality in reviewed regions	Independent documents for transfer

Table 7. Recorded CLIP revision runtime in seconds. Full processing covers six pages; incremental processing changes page 10 and reuses five pages.

Stage	Full	Incremental
Composition	65.75	9.65
Preflight	24.17	23.03
Complete finalization	93.74	37.11

5.5 Visual Case: Mathematics in Ordinary Fonts

The visual case supplies evidence complementary to object counts. The earlier engine creates zero formula objects and visibly wraps the display equation. Version 0.4.1 creates two formula objects and retains source geometry. Inline variables differ less dramatically at thumbnail scale, so object inventories and readable-resolution crops are both necessary. The underlying reusable conditions ask whether a span uses an ordinary italic font, whether it forms a bounded algebraic relation, and whether an isolated letter has nearby mathematical context on the same line. These conditions can be tested across fonts and positions without depending on a document name or page number.

5.6 Bounded Native Restoration

When the source formula remains intact, native restoration reduces the uncertainty introduced by OCR or formula regeneration. The repair interface requires a one-to-one source/output mapping, equal-scale bilingual panels, and a source region contained by an explicit clearing region. For render operator R_r at resolution r, the checks are

$$R_{288}(\text{source clip}) = R_{288}(\text{restored clip}), \tag{5}$$

$$R_{144}(\text{before}, \Omega^c) = R_{144}(\text{after}, \Omega^c), \tag{6}$$

where Ω is the declared edit region with a 0.5-pt antialiasing mask at its boundary. All eight cases pass both checks, covering 16 page-level outside-region comparisons.

6. Document-Level Case Studies

Historical document work spans multiple evidence scopes. A 51-page technical report was reviewed around specified high-impact issues; a 30-page mathematical report received full-page

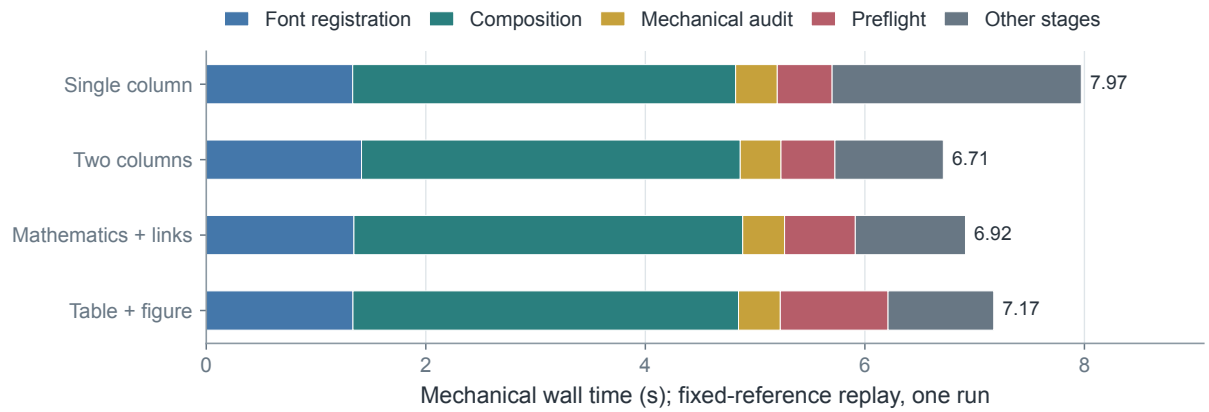


Figure 7. Mechanical-layout wall time for four normal version-0.4.1 fixtures. Each bar is one sequential run with fixed target text. Language generation, diagnosis, host repair, and final review are recorded separately.

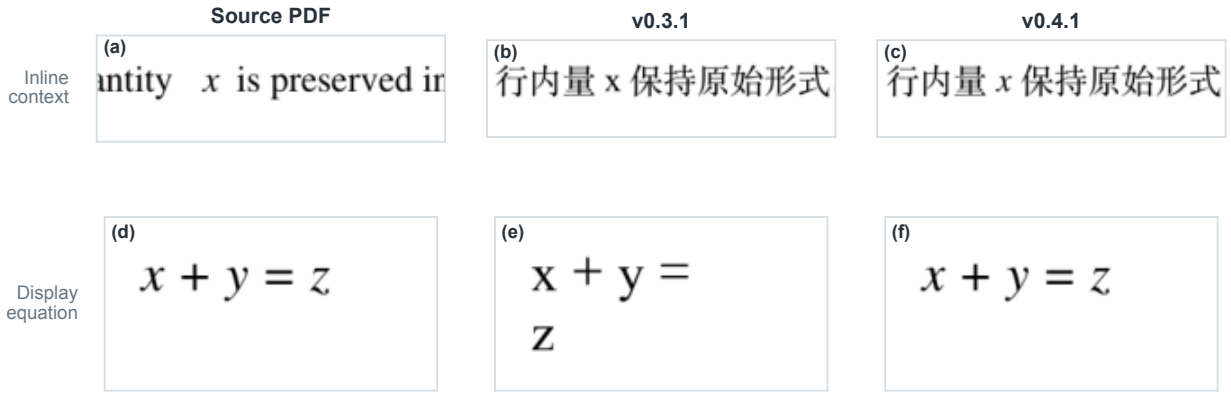


Figure 8. Rendered crops from the source and two engine versions. Version 0.3.1 treats the standalone equation as ordinary text and reflows it. Version 0.4.1 preserves the native PDF glyphs and layout.

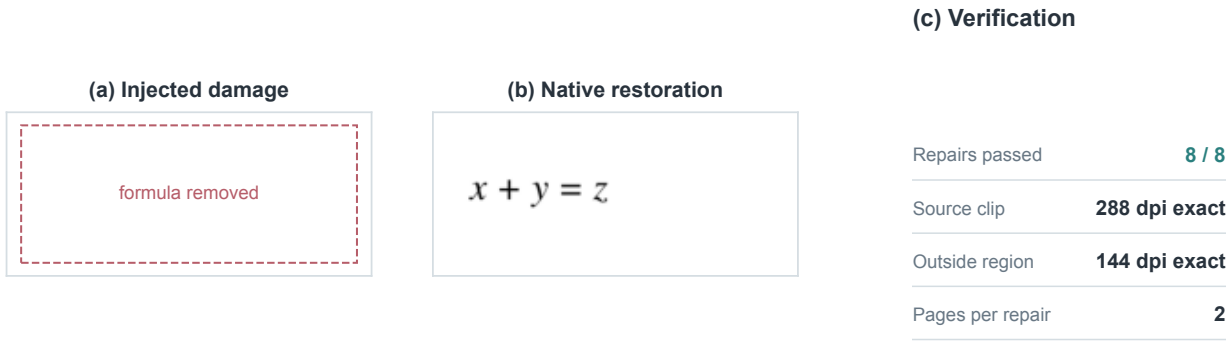


Figure 9. Damage injection, restoration from the native source PDF, and verification. Eight trials cover four font sizes and two page widths.

Table 8. Restoration constraints and tested scope.

Constraint	Tested scope	Extension
Page geometry	Two pages, equal-scale panels	Continuations and unequal panels require a second protocol
Native formula	8/8 at 288 dpi	Given source region
Outside region	16 pages at 144 dpi	0.5-pt boundary mask
Task state	Separate candidate and proof	Independent validation status

review; later CBD and AIGB documents focused on titles, captions, appendices, and reported regions. These materials drove different system layers: extraction and formula ownership entered the engine, interruption recovery entered the workflow, visual inspection and source coverage entered the skill instructions, and bounded region restoration remained attached to document-specific candidates.

Because the review protocols differ, we treat these artifacts as traceable cases rather than pool their page counts into a single accuracy estimate. Their value lies in identifying recurring mechanisms and establishing the provenance of later regression tests.

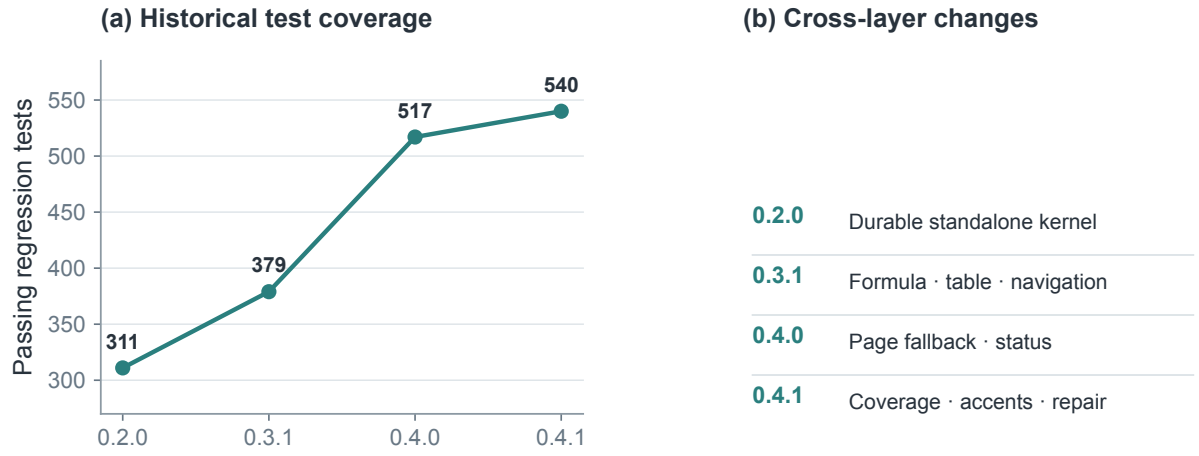


Figure 10. Engineering progression recorded in historical acceptance runs. Test counts reflect expanding regression coverage; document accuracy and semantic quality use separate evaluations.

Table 9. Scope of historical document evidence.

Document	Recorded scope	Supported conclusion
DeepSeek technical report	v0.3.1; 51 pages; 353 current entries	Revision acceptance for specified major issues
DeepSeekMath	v0.4.0; 30 pages; 161 entries; full-page review	Complete example delivery with a retained source navigation issue
CBD	v0.4.1; 23 pages; 115 entries	Review of titles, captions, appendices, and reported regions
AIGB	v0.4.1; 12 pages	Multiple regions and page-12 revision; remaining style findings recorded
GAVE	Formula on page 5 of an 11-page draft	Local restoration of one formula and its explanation

Candidate availability and visual verification. On DDPM page 7, a collision check initially rejected the translated layout because the protected region around Figure 7 intersected its caption region. The resulting source-only output prevented inspection of the translated candidate. After the workflow was changed to retain translated content despite quality findings, visual review found no visible obstruction corresponding to that warning. Subsequent local repairs addressed mathematical glyphs and citation wrapping. This case motivated separate states for candidate availability and acceptance, together with visual review of the actual artifact. The final output appears in Appendix C. The source-only fallback recorded in the version-replay tables belongs to the earlier workflow evaluated in those experiments.

List structure across fragmented text blocks. On AIGB page 5, inline mathematics split a numbered list across extraction blocks. The initial translation merged two items and lost bold labels and hanging indentation. The engine update grouped fragments by item, retained label weight, and aligned continuation lines with the body text to the right of the marker. Regression checks and visual inspection of the regenerated page supported the correction. This case illustrates how a visible formatting defect can be traced to structural extraction and converted into a reusable layout rule; Appendix C shows the corrected output.

Caption coverage and object ownership. TIGER extraction failures exposed table captions excluded by a preservation rule, fragmented subfigure captions, and numbered URL footnotes that lost their source arrangement. The resulting rules separate captions from table cells, join complete subcaptions using relative geometry, recover bullet structure from native symbols, and preserve URL-footnote blocks. Recorded re-extraction placed six table captions in the translation catalog and recovered complete subcaptions and three research-question items. A fresh regression job verified that normal composition translated a table caption while retaining table data. Additional regressions cover bold caption continuations misclassified as headings and chart digits incorrectly reassigned to neighboring prose. These cases connect ownership and reading-order errors to reusable extraction rules.

The focused supporting suite passed 54 tests spanning incremental revision, translation-prevention rules, independent source coverage, terminology and reading context, caption flow, and grouped translation. It includes fresh-job composition, unchanged-page equivalence, and invalid-cache fallback. These checks establish the tested implementation behaviors; document-level semantic quality is assessed through the evaluation protocol in Section 7.

6.1 Geometry, Object Ownership, and Source Coverage

We repeatedly processed physical pages 4, 5, and 8 of TimesNet to examine three interacting mechanisms: source-aligned

geometry, ownership of graphical and mathematical objects, and completeness of source extraction. Each observed failure informed an engine revision, and the resulting artifacts preserve the connection between diagnosis, implementation, and visible output.

Page 4 shows that header rules, equation placement, line spacing, heading baselines, and panel gutters are deterministic layout invariants. Moving them into the manifest and preflight turns a recurring reconstruction task into mechanical behavior. Page 5 exposes a shared object-ownership problem: diagram labels belong to the diagram, SVG glyph visibility depends on inherited clipping, and prose removal must use concrete glyph identity rather than oversized font metrics. The resulting clipping and cleanup mechanisms pass the regression suite and a clean replay of the same page.

Page 8 marks a different boundary. Layout and preflight pass, yet a complex figure-text wrap causes classification results and the caption to enter a preserved compound object. Issued-entry completion therefore coexists with incomplete source coverage. The host repair recovers three regions while preserving the table and chart labels. This case motivates a general extraction rule for complex wraps and reinforces the need to verify source coverage independently of catalog and layout status.

7. Protocol for Strict Validation and Attribution

Deliberately selected training samples. During skill self-evolution, we used five challenging pages from four papers as development training samples: TimesNet page 4, RankMixer page 7, AIGB pages 5 and 7, and DDPM page 7. These pages were deliberately selected for their demanding combinations of mathematical notation, figures, tables, and multi-column text. Here, training consists of iterative task execution, user feedback, diagnosis, and updates to the skill's instructions and executable mechanisms. The samples expose complementary problems, including formula placement, dense table boundaries, numbered-list structure, subplot labels, and native mathematical glyphs embedded in prose. Appendix C reproduces the final bilingual outputs. Their role in candidate development determines their placement in the development partition of the evaluation protocol below.

Candidate versions should be frozen before documents are grouped by source and template similarity into development, validation, and final-test partitions. Pages from the same paper, small variants of one template, and probes derived from them share one group identity. Once a test failure influences a change, that document joins the development history; future transfer evaluation uses a new source.

To separate instruction effects from engine effects, the four cells in Fig. 11 combine old and new instructions with old and new engines while holding the host model, reasoning configuration, tools, input, and clean-session conditions fixed. Repeated stochastic runs are aggregated by document. Letting $Q(S, C)$ denote the declared quality vector under instructions S and engine C, the instruction effect at a fixed engine is

$$\Delta_S Q = Q(S_{\text{new}}, C_{\text{fixed}}) - Q(S_{\text{old}}, C_{\text{fixed}}). \tag{7}$$

A complementary host-model comparison should hold the skill, engine, documents, tools, and review policy fixed while varying the vision-capable model. Report semantic quality, source coverage, visible defects, repair success, token usage, and elapsed delivery time across repeated runs. A shared-target-text condition can isolate review and repair differences, while an end-to-end condition measures the combined effects of translation generation and subsequent inspection. This comparison tests the expectation of limited layout variation under a common deterministic engine. Critical source coverage, mathematical integrity, numerical correctness, and readable layout are treated as hard constraints. Semantic accuracy, repaired-page count, intervention count, and total delivery cost are compared after those constraints hold. The final report uses sealed test documents and records model versions and repetition conditions.

8. Limitations and Discussion

The controlled mechanism evidence comes from four normal fixtures and 48 probes constructed around known failure families. It supports the corresponding conditional rules; broader PDF transfer requires a larger, source-independent document collection. Cross-version replay evaluates whole systems, while the targeted ablations isolate only two recognition paths. Fixed target text controls language generation, so semantic translation quality belongs to the model-level experiment proposed above.

Native restoration results apply to the recorded page mappings, crop boxes, renderers, and resolutions. Historical cases also combine user selection, document difficulty, and accumulated engineering experience. The TimesNet pages are part of the development history. Comparisons with SkillOpt or GEPA under a common task harness, automated causal routing, cross-viewer rendering consistency, and document-level held-out evaluation are natural next steps.

Real use and controlled evidence play complementary roles. User feedback surfaces reading failures that automated scores have not yet modeled; controlled replay makes version and mechanism effects comparable. Over time, task evidence can produce candidate rules, regression tests, and new document-level experiments. Much of the scientific work lies in defining the failure, selecting the mechanism, and choosing a verification target that supports the intended claim.

9. Conclusion

SkillWeave treats a scientific-PDF skill as a coordinated system of instructions, executable mechanisms, workflow state, and verification. Version replay, mechanism probes, ablation, and native-restoration trials establish concrete improvements in ordinary-font mathematical recognition and bounded repair. The longitudinal cases clarify the division of labor: instructions govern decisions, code implements clipping, ownership, and geometry, workflow state makes recovery durable, and independent source coverage catches omissions beyond issued catalogs. Reusable skill improvement follows when local document evidence is abstracted into stable mechanisms and every claim remains connected to an inspectable artifact.

References

BabelDOC contributors. BabelDOC: PDF scientific paper translation and bilingual comparison library. Open-source software. https://github.com/funstory-ai/

Table 10. Longitudinal TimesNet development cases. Wall-clock intervals come from the recorded run scopes; all pages share one document identity.

Case	Observed requirement or failure	Update and result
Page 4; five clean replays	Header rule, display-equation position, body leading, section-heading baseline, and bilingual gutter	Source anchors became hard layout checks. The gutter contracted from 213.0 to 106.5 pt at source scale. Final mechanical output took 133.88 s; one review brought the interval to 206.15 s.
Page 5; initial delivery	Diagram-label collisions, hidden clipped English glyphs in formulas, and source letters beneath target prose	The first mechanical segment took 185.91 s, followed by three host candidates and a 1218.29-s delivery window. Candidate generation accounted for a small recorded portion; diagnosis and repair authoring dominated the unsegmented time.
Page 5; engine update	Promote diagram ownership, SVG clipping, and glyph cleanup into reusable mechanisms	The auto policy preserved diagram labels, inherited transforms and clipping were retained, and prose cleanup used glyph identity. Exact-source target reuse produced a complete mechanical draft in 97.36 s; final mechanical replay took 60.31 s with no host PDF repair.
Page 8; coverage case	4/4 issued entries submitted and layout certified while classification results and a figure caption were merged into a preserved object	Visual source coverage split the material into three target regions. The mechanical draft arrived in 96.60 s; the delivery including supplementation and review took 577.24 s.

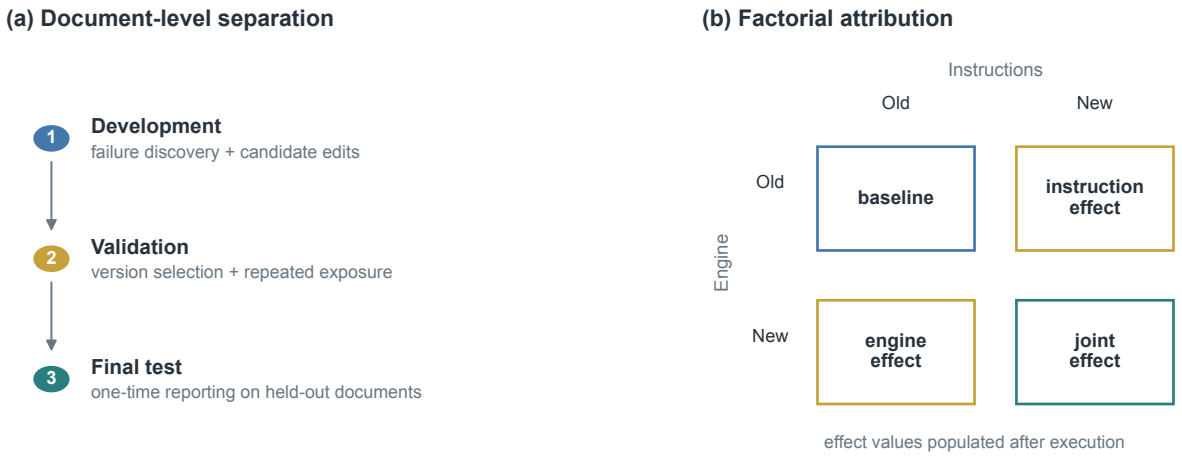


Figure 11. Planned evaluation protocol. Documents are separated by source and template family. A 2×2 design then isolates instruction and engine effects under a fixed host model and execution environment.

BabelDOC. Accessed October 26, 2026.

Y. Yang et al. SkillOpt: Executive Strategy for Self-Evolving Agent Skills. *arXiv:2605.23904*, 2026.

L. A. Agrawal et al. GEPA: Reflective Prompt Evolution Can Outperform Reinforcement Learning. *arXiv:2507.19457*, 2025.

M. Yuksekgonul et al. TextGrad: Automatic Differentiation via Text. *arXiv:2406.07496*, 2024.

X. Li et al. SkillsBench: Benchmarking How Well Agent Skills Work Across Diverse Tasks. *arXiv:2602.12670*, 2026.

S. Alzubi et al. EvoSkill: Automated Skill Discovery for Multi-Agent Systems. *arXiv:2603.02766*, 2026.

S. Shen et al. SkillFoundry: Building Self-Evolving Agent Skill Libraries from Heterogeneous Scientific Resources. *arXiv:2604.03964*, 2026.

A. Evidence Index and Reproduction

All experimental figures are generated from measured data or explicitly identified historical records. The concept figures and the proposed attribution protocol describe methods and planned cells. The project includes vector PDF/SVG figures, PNG previews, the structured article source, replay reports, probe manifests, restoration proofs, and the continuous-task record.

Table 11. Evidence files distributed with the research package.

Material	Location	Purpose
Versions and commands	`evidence/provenance.json`	Wheel hashes, interpreter, and commands
Cross-version replay	`evidence/replay/<version>/report.json`	Outputs and diagnostics for 24 tasks
Probes and labels	`evidence/probe-manifest.json`	Forty-eight PDFs, labels, and hashes
Extraction and ablation	`evidence/probes-results/`	336 recognition records and module paths
Restoration proof	`evidence/repair-study.json`	Candidate hashes and checked regions
Continuous cases	`evidence/continuous-task-case.json`	Page 4/5/8 traces, timings, hashes, and scope
Regression records	`evidence/pytest.xml`; `continuous-regression.xml`	Complete test-suite results
Editable figures	`figures/`; `scripts/make_figures.py`	Rebuildable vector figures

The original study regression contains 540 passing tests. The later continuous-task engine update contains 572 passing tests. Replays copy each historical wheel or source snapshot into an isolated directory and set `PYTHONPATH` accordingly. New runs

should use fresh output directories so that recorded evidence remains immutable.

Supporting implementation evidence is distributed in `evidence/`: `incremental-layout-benchmark.json` contains the CLIP revision timings; `pipeline-regressions.xml` records the 54 focused checks; and `implementation-provenance.json` binds those checks to source-file hashes. The historical experiment records and the supporting implementation checks retain their separate run configurations.

B. Runtime Fingerprints

The exact engine fingerprints for versions 0.2.0, 0.3.1, 0.4.0, and 0.4.1 are stored in `evidence/provenance.json`. Source and output hashes for the TimesNet page sequence are stored in `evidence/continuous-task-case.json`.

C. Training Samples Used During Skill Self-Evolution

Figures 12–16 show the final outputs for the five deliberately selected development training samples in Section 7. Each complete image places the English source on the left and the Chinese translation on the right. The pages concentrate difficult formulas, figures, tables, and layout structures. Images were rendered from the delivered PDFs at 300 dpi; the accompanying manifest records page mappings and artifact hashes.

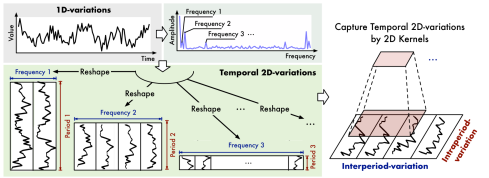


Figure 2: A univariate example to illustrate 2D structure in time series. By discovering the periodicity, we can transform the original 1D time series into structured 2D tensors, which can be processed by 2D kernels conveniently. By conducting the same reshape operation to all variates of time series, we can extend the above process to multivariate time series.

Here, $\mathrm{FFT}(\cdot)$ and $\mathrm{Amp}(\cdot)$ denote the FFT and the calculation of amplitude values. $\mathbf{A} \in \mathbb{R}^T$ represents the calculated amplitude of each frequency, which is averaged from C dimensions by $\mathrm{Avg}(\cdot)$. Note that the j-th value $\mathbf{A}_j$ represents the intensity of the frequency-j periodic basis function, corresponding to the period length $\lceil \frac{T}{j} \rceil$. Considering the sparsity of frequency domain and to avoid the noises brought by meaningless high frequencies (Chatfield, 1981; Zhou et al., 2022), we only select the top-k amplitude values and obtain the most significant frequencies $\{f_1, \cdots, f_k\}$ with the unnormalized amplitudes $\{\mathbf{A}_{f_1}, \cdots, \mathbf{A}_{f_k}\}$, where k is the hyper-parameter. These selected frequencies also correspond to k period lengths $\{p_1, \cdots, p_k\}$. Due to the conjugacy of frequency domain, we only consider the frequencies within $\{1, \cdots, \lfloor \frac{T}{2} \rfloor\}$. We summarize Equation 1 as follows:

$$\mathbf{A}, \{f_1, \cdots, f_k\}, \{p_1, \cdots, p_k\} = \mathrm{Period}(\mathbf{X}_{1\mathrm{D}}). \tag{2}$$

Based on the selected frequencies $\{f_1, \cdots, f_k\}$ and corresponding period lengths $\{p_1, \cdots, p_k\}$, we can reshape the 1D time series $\mathbf{X}_{1\mathrm{D}} \in \mathbb{R}^{T \times C}$ into multiple 2D tensors by the following equations:

$$\mathbf{X}^i_{2\mathrm{D}} = \mathrm{Reshape}_{p_i, f_i}\left(\mathrm{Padding}(\mathbf{X}_{1\mathrm{D}})\right), \ i \in \{1, \cdots, k\}, \tag{3}$$

where $\mathrm{Padding}(\cdot)$ is to extend the time series by zeros along temporal dimension to make it compatible for $\mathrm{Reshape}_{p_i, f_i}(\cdot)$, where p_i and f_i represent the number of rows and columns of the transformed 2D tensors respectively. Note that $\mathbf{X}^i_{2\mathrm{D}} \in \mathbb{R}^{p_i \times f_i \times C}$ denotes the i-th reshaped time series based on frequency-f_i, whose columns and rows represent the intraperiod-variation and interperiod-variation under the corresponding period length p_i respectively. Eventually, as shown in Figure 2, based on the selected frequencies and estimated periods, we obtain a set of 2D tensors $\{\mathbf{X}^1_{2\mathrm{D}}, \cdots, \mathbf{X}^k_{2\mathrm{D}}\}$, which indicates k different temporal 2D-variations derived by different periods.

It is also notable that, this transformation brings two types of localities to the transformed 2D tensors, that is localities among adjacent time points (columns, intraperiod-variation) and adjacent periods (rows, interperiod-variation). Thus, the temporal 2D-variations can be easily processed by 2D kernels.

3.2 TimesBlock

As shown in Figure 3, we organize the TimesBlock in a residual way (He et al., 2016). Concretely, for the length-T 1D input time series $\mathbf{X}_{1\mathrm{D}} \in \mathbb{R}^{T \times C}$, we project the raw inputs into the deep features $\mathbf{X}^0_{1\mathrm{D}} \in \mathbb{R}^{T \times d_{\mathrm{model}}}$ by the embedding layer $\mathbf{X}^0_{1\mathrm{D}} = \mathrm{Embed}(\mathbf{X}_{1\mathrm{D}})$ at the very beginning. For the l-th layer of TimesNet, the input is $\mathbf{X}^{l-1}_{1\mathrm{D}} \in \mathbb{R}^{T \times d_{\mathrm{model}}}$ and the process can be formalized as:

$$\mathbf{X}^l_{1\mathrm{D}} = \mathrm{TimesBlock}\left(\mathbf{X}^{l-1}_{1\mathrm{D}}\right) + \mathbf{X}^{l-1}_{1\mathrm{D}}. \tag{4}$$

As shown in Figure 3, for the l-th TimesBlock, the whole process involves two successive parts: capturing temporal 2D-variations and adaptively aggregating representations from different periods.

Capturing temporal 2D-variations Similar to Equation 1, we can estimate period lengths for deep features $\mathbf{X}^{l-1}_{1\mathrm{D}}$ by $\mathrm{Period}(\cdot)$. Based on estimated period lengths, we can transform the 1D time series

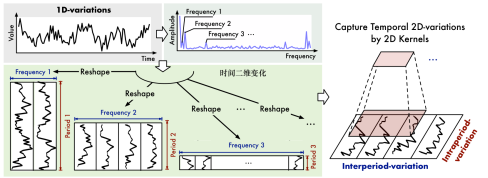


图 2：以单变量示例说明时间序列中的二维结构。通过发现周期性，我们可以将原始一维时间序列转换为具有结构的二维张量，从而方便地使用二维卷积核处理。对时间序列的所有变量执行相同的重塑操作，即可将上述过程扩展到多变量时间序列。

这里，$\mathrm{FFT}(\cdot)$ 和 $\mathrm{Amp}(\cdot)$ 分别表示 FFT 和幅值计算。$\mathbf{A} \in \mathbb{R}^T$ 表示计算得到的各频率的幅值，它由 C 个维度通过 $\mathrm{Avg}(\cdot)$ 取平均得到。注意，第 j 个值 $\mathbf{A}_j$ 表示频率为 j 的周期基函数的强度，其对应的周期长度为 $\lceil \frac{T}{j} \rceil$。考虑到频域的稀疏性，并为避免无意义的高频引入噪声 (Chatfield, 1981; Zhou et al., 2022)，我们仅选择幅值最大的 k 个值，并得到最显著的频率 $\{f_1, \cdots, f_k\}$ 及其未归一化幅值 $\{\mathbf{A}_{f_1}, \cdots, \mathbf{A}_{f_k}\}$，其中 k 是超参数。这些选定的频率也对应于 k 个周期长度 $\{p_1, \cdots, p_k\}$。由于频域的共轭性，我们仅考虑 $\{1, \cdots, \lfloor \frac{T}{2} \rfloor\}$ 范围内的频率。我们将公式 1 概括如下：

$$\mathbf{A}, \{f_1, \cdots, f_k\}, \{p_1, \cdots, p_k\} = \mathrm{Period}(\mathbf{X}_{1\mathrm{D}}). \tag{2}$$

根据选定的频率 $\{f_1, \cdots, f_k\}$ 及对应的周期长度 $\{p_1, \cdots, p_k\}$，我们可以通过以下公式，将一维时间序列 $\mathbf{X}_{1\mathrm{D}} \in \mathbb{R}^{T \times C}$ 重塑为多个二维张量：

$$\mathbf{X}^i_{2\mathrm{D}} = \mathrm{Reshape}_{p_i, f_i}\left(\mathrm{Padding}(\mathbf{X}_{1\mathrm{D}})\right), \ i \in \{1, \cdots, k\}, \tag{3}$$

其中，$\mathrm{Padding}(\cdot)$ 沿时间维度对时间序列补零，使其适用于 $\mathrm{Reshape}_{p_i, f_i}(\cdot)$，而 p_i 和 f_i 分别表示转换后的二维张量的行数和列数。注意，$\mathbf{X}^i_{2\mathrm{D}} \in \mathbb{R}^{p_i \times f_i \times C}$ 表示第 i 个基于频率 f_i 重塑得到的时间序列，其列和行分别表示对应周期长度 p_i 下的周期内变化和周期间变化。最终，如图 2 所示，根据选定的频率和估计的周期，我们得到一组二维张量 $\{\mathbf{X}^1_{2\mathrm{D}}, \cdots, \mathbf{X}^k_{2\mathrm{D}}\}$，它表示由不同周期导出的 k 种不同的时间二维变化。

还值得注意的是，这种转换为转换后的二维张量引入了两类局部性，即相邻时间点之间的局部性（列，周期内变化）和相邻周期之间的局部性（行，周期间变化）。因此，时间二维变化可以很容易地用二维卷积核处理。

3.2 TIMESBLOCK

如图 3 所示，我们以残差方式组织 TimesBlock (He et al., 2016)。具体而言，对于长度为 T 的一维输入时间序列 $\mathbf{X}_{1\mathrm{D}} \in \mathbb{R}^{T \times C}$，我们首先将原始输入投影为深层特征 $\mathbf{X}^0_{1\mathrm{D}} \in \mathbb{R}^{T \times d_{\mathrm{model}}}$，这由嵌入层 $\mathbf{X}^0_{1\mathrm{D}} = \mathrm{Embed}(\mathbf{X}_{1\mathrm{D}})$ 完成。对于 TimesNet 的第 l 层，输入为 $\mathbf{X}^{l-1}_{1\mathrm{D}} \in \mathbb{R}^{T \times d_{\mathrm{model}}}$，其过程可形式化为：

$$\mathbf{X}^l_{1\mathrm{D}} = \mathrm{TimesBlock}\left(\mathbf{X}^{l-1}_{1\mathrm{D}}\right) + \mathbf{X}^{l-1}_{1\mathrm{D}}. \tag{4}$$

如图 3 所示，对于第 l 个 TimesBlock，整个过程包括两个连续的部分：捕获时间二维变化，以及自适应聚合不同周期的表征。

捕获时间二维变化 与公式 1 类似，我们可以估计深层特征 $\mathbf{X}^{l-1}_{1\mathrm{D}}$ 的周期长度，所用方法为 $\mathrm{Period}(\cdot)$。根据估计的周期长度，我们可以将一维时间序列转换

Figure 12. TimesNet, source page 4: final bilingual output used as a development training sample. The page combines a temporal-variation diagram, inline mathematical notation, and three display equations. It supported refinements to formula anchors, line spacing, and source-aligned layout.

Table 4: Online AB test result for Feed Recommendation Scenarios in both Douyin and Douyin lite app and the improvements are all statistically significant. According to long-term reverse A/B tests and continuous observations over long-term reverse experiments, the gains provided by RankMixer-1B have not yet converged, and the results presented here are still improving.

	Douyin app					Douyin lite				
	Active Day↑	Duration↑	Like↑	Finish↑	Comment↑	Active Day↑	Duration↑	Like↑	Finish↑	Comment↑
Overall	+0.2908%	+1.0836%	+2.3852%	+1.9874%	+0.7886%	+0.1968%	+0.9869%	+1.1318%	+2.0744%	+1.1338%
Low-active	+1.7412%	+3.6434%	+8.1641%	+4.5393%	+2.9368%	+0.5389%	+2.1831%	+4.4486%	+3.3958%	+0.9595%
Middle-active	+0.7081%	+1.5269%	+2.5823%	+2.5062%	+1.2266%	+0.4235%	+1.9011%	+1.7491%	+2.6568%	+0.6782%
High-active	+0.1445%	+0.6259%	+1.828%	+1.4939%	+0.4151%	+0.0929%	+1.1356%	+1.8212%	+1.7683%	+2.3683%

Table 5: Online lift of RankMixer in Advertising

	Advertising	
Metric	ΔAUC↑	ADVV↑
Lift	+0.73%	+3.90%

Table 6: Metrics of Online Model Deployment and Cost

Metric	OnlineBase-16M	RankMixer-1B	Change
#Param	15.8M	1.1B	↑ **70×**
FLOPs	107G	2106G	↑ 20.7×
Flops/Param(G/M)	6.8	1.9	↓ 3.6×
MFU	4.47%	**44.57%**	↑ 10×
Hardware FLOPs	fp32	fp16	↑ 2×
Latency	14.5ms	**14.3ms**	-

Expert balance and diversity. Vanilla Sparse MoE often suffers from expert imbalance, which in turn leaves some experts under-trained and eventually leads to "dying experts" (experts that are almost never activated) and only a few fixed experts are constantly activated. Figure 4 shows that combining DTSI (dense-training, sparse-inference) with ReLU routing effectively resolves this issue: Dense-training guarantees that most expert receives sufficient gradient updates, preventing expert starvation. ReLU routing makes the activation ratio dynamic across tokens—the activation proportion shows in the figure varies adaptively according to its information content, which aligns well with the diverse and highly dynamic distribution of recommendation data.

4.6 Online Serving cost

How can we prevent inference latency from exploding with a two-order-of-magnitude increase in parameters? In practical systems, latency is inversely proportional to throughput and directly proportional to the cost of serving machine resources. Compared to our previous fully-deployed 16M-parameter model (with a structure integrated with DLRM and DCN), our RankMixer model scaled parameters by approximately 70× to 1B. Despite this significant parameter increase, the final inference latency remained stable due to our hardware-aligned model design and optimization strategies.

When greatly increasing model parameters, latency can be decomposed into the following formula:

$$\text{Latency} = \frac{\text{\#Param} \times \text{FLOPs/Param ratio}}{\text{MFU} \times (\text{Theoretical Hardware FLOPs})}$$

As illustrated in Table 6, the two-order-of-magnitude parameter increase is progressively counteracted by **3.6×** decrease of FLOPs/Param ratio, **10** × increase of MFU and Quatization-based **2** × Hardware FlOPs improvements.

(1) **FLOPs/Param ratio.** The three row of Table 6 reports the number of floating-point operations (FLOPs) required *per parameter*. Thanks to the model design, RankMixer achieves a 70-fold increase in parameters with only around a 20-fold increase in FLOPs, achieving only one-third the FLOPs/Param ratio of the baseline—a **3.6,× efficiency gain**. In other words, RankMixer can accommodate three times more parameters than the baseline at the same FLOPs budget.
(2) **Model FLOPs Utilization (MFU).** Also shown in Table 6, MFU indicates the utilization of machine computing. By using large GEMM shapes, good parallel topology (fusing parallel per-token FFNs into one kernel), reduce the memory bandwith cost and overhead, RankMixer raises MFU by nearly **10** ×, shifting the model from an *Memory-bound* to a *Compute-bound* regime.
(3) **Quantization** Half-precision (fp16) inference will increase the theoretical peak Hardware FLOPS of GPUs by **2** ×.The primary computations in RankMixer consist of several large matrix multiplications that are well suited for half-precision (fp16) inference as mentioned before

4.7 Online Performance

To verify the universality of RankMixer as a scaling recommendation model framework, we conducted online experiments in the two core application scenarios of personalised ranking—*feed recommendation* and *advertising*, covering major use-cases of personalized ranking. For each scenario we monitor the following key performance indicators:

- **Feed–Recommendation.** *Active Days* is he average number of active days per user during the experiment period, a substitute for DAU growth.; *Duration* measures cumulative stay time on the App; *Finish/Like/Comment:* User's total complete plays, likes, and comments.
- **Advertising.** We report the model quality metrics (Δ*AUC*) and revenue metrics *ADVV* (Advertiser Value).

The Previous baselines in these scenarios are 16M parameter model combined with DLRM and DCN. We replaced the Dense part with the RankMixer-1B model improving a 0.7% AUC. We conduct online A/B test experiments across Feed Recommendation and Advertising. The long-term observation of A/B test result on

Table 4: Online AB test result for Feed Recommendation Scenarios in both Douyin and Douyin lite app and the improvements are all statistically significant. According to long-term reverse A/B tests and continuous observations over long-term reverse experiments, the gains provided by RankMixer-1B have not yet converged, and the results presented here are still improving.

	Douyin app					Douyin lite				
	Active Day↑	Duration↑	Like↑	Finish↑	Comment↑	Active Day↑	Duration↑	Like↑	Finish↑	Comment↑
Overall	+0.2908%	+1.0836%	+2.3852%	+1.9874%	+0.7886%	+0.1968%	+0.9869%	+1.1318%	+2.0744%	+1.1338%
Low-active	+1.7412%	+3.6434%	+8.1641%	+4.5393%	+2.9368%	+0.5389%	+2.1831%	+4.4486%	+3.3958%	+0.9595%
Middle-active	+0.7081%	+1.5269%	+2.5823%	+2.5062%	+1.2266%	+0.4235%	+1.9011%	+1.7491%	+2.6568%	+0.6782%
High-active	+0.1445%	+0.6259%	+1.828%	+1.4939%	+0.4151%	+0.0929%	+1.1356%	+1.8212%	+1.7683%	+2.3683%

Table 5: Online lift of RankMixer in Advertising

	Advertising	
Metric	ΔAUC↑	ADVV↑
Lift	+0.73%	+3.90%

Table 6: Metrics of Online Model Deployment and Cost

Metric	OnlineBase-16M	RankMixer-1B	Change
#Param	15.8M	1.1B	↑ **70×**
FLOPs	107G	2106G	↑ 20.7×
Flops/Param(G/M)	6.8	1.9	↓ 3.6×
MFU	4.47%	**44.57%**	↑ 10×
Hardware FLOPs	fp32	fp16	↑ 2×
Latency	14.5ms	**14.3ms**	-

专家均衡与多样性。原始的稀疏 MoE 常常存在专家失衡问题，导致部分专家训练不足．最终出现"死亡专家"（几乎从不被激活的专家），而始终被激活的只有少数固定专家。图 4 表明，将 DTSI（稠密训练、稀疏推理）与 ReLU 路由结合，能够有效解决这一问题：稠密训练保证大多数专家获得充分的梯度更新，避免专家"饥饿"。ReLU 路由使激活比例随 token 动态变化——图中所示的激活比例会根据信息内容自适应调整，与推荐数据多样且高度动态的分布十分契合。

4.6 在线服务成本

当参数量增加两个数量级时，如何避免推理延迟激增？在实际系统中，延迟与吞吐量成反比，与在线服务所需机器资源的成本成正比。与我们此前已全面部署的 1600 万参数模型（其结构融合了 DLRM 和 DCN）相比，RankMixer 的参数量扩展至约 70×，达到 10 亿。尽管参数量显著增加，但得益于贴合硬件的模型设计和优化策略，最终的推理延迟仍保持稳定。

当模型参数量大幅增加时，延迟可分解为如下公式：

$$\text{Latency} = \frac{\text{\#Param} \times \text{FLOPs/Param ratio}}{\text{MFU} \times (\text{Theoretical Hardware FLOPs})}$$

如表 6 所示，参数量增加两个数量级所带来的影响，被 FLOPs/Param 比值降低 **3.6**×、MFU 提升 **10**×，以及量化带来的硬件 FLOPs 提升 **2**× 逐步抵消。

(1) **FLOPs/Param 比值**：表 6 的第三行给出了每个参数所需的浮点运算次数（FLOPs）。
得益于模型设计，RankMixer 在参数量增至 70 倍的同时，FLOPs 仅增至约 20 倍，FLOPs/Param 比值仅为基线的三分之一，实现了 **3.6,**× 的效率提升。换言之，在相同的 FLOPs 预算下，RankMixer 可容纳基线三倍的参数量。

(2) **模型浮点运算利用率（MFU）**：如表 6 所示，MFU 表示机器计算能力的利用率。通过采用大尺寸 GEMM、良好的并行拓扑（将各 token 的并行 FFN 融合为一个内核），并降低内存带宽成本和开销，RankMixer 将 MFU 提升了近 **10**×，使模型从受内存带宽限制转变为受计算能力限制。

(3) **量化**：半精度（fp16）推理可使 GPU 的理论峰值硬件 FLOPS 提升 **2**×。如前所述，RankMixer 的主要计算由若干大型矩阵乘法组成，非常适合采用半精度（fp16）推理。

4.7 在线效果

为验证 RankMixer 作为推荐模型规模扩展框架的通用性，我们在个性化排序的两个核心应用场景——信息流推荐和广告——中开展了在线实验，覆盖个性化排序的主要用例。对于每个场景，我们监测以下关键性能指标：

- **信息流推荐**。Active Days 指实验期间每位用户的平均活跃天数，是 DAU 增长的替代指标；Duration 衡量用户在 App 中的累计停留时长；Finish/Like/Comment 分别表示用户完整播放、点赞和评论的总次数。
- **广告**。我们报告模型质量指标（ΔAUC）以及收益指标 ADVV（广告主价值）。

这些场景此前的基线均为结合 DLRM 和 DCN 的 1600 万参数模型。我们用 RankMixer-1B 模型替换其中的稠密部分，使 AUC 提升了 0.7%。我们在信息流推荐和广告场景开展在线 A/B 测试。对 A/B 测试结果的长期观察表明，

Figure 13. RankMixer, source page 7: final bilingual output used as a development training sample. Three performance tables coexist with a latency formula, numbered explanations, and separate application scenarios. The final output retains the native tables and restores the structure of the scenario list.

4.3 Design of Conditions.

In this section, we present approaches transforming industrial metrics into conditions of DiffBid.

4.3.1 ***Generation with Returns***. For each trajectory τ we have the total value the advertiser received as the the return $R(\tau) = \sum_{t=1}^{T} r_t$. We normalize the return by:

$$R = \frac{R(\tau) - R_{\min}}{R_{\max} - R_{\min}}, \tag{13}$$

where $R_{\min}$ and $R_{\max}$ are the smallest and the largest return in the dataset. Through Eq. 13 we normalize the return into $[0, 1]$ and merge it into $y(\tau)$. Subsequently, we train the model to generate trajectories conditioned on the normalized returns. It should be noted that trajectories with more values received have higher normalized returns. Thus $R = 1$ indicates the best trajectory with the highest values which will better fit the advertisers' needs. When generation, we just set $R = 1$ and generate the trajectory under the max return condition to the advertiser.

4.3.2 ***Generation with Constraints or Human Feedback***. In MCB, the cumulative performance related to the constraints within a given episode should be controlled so as not to exceed the advertisers' expectations. In such a setting, we can design $\boldsymbol{y}(\tau)$ to control the generation process. For example, in the Target-CPC setting, we can maintain a binary variable E to indicate whether the final CPC exceeds the given constraint C:

$$E = \mathrm{I}_{x \le C}(x) \tag{14}$$

where $x = \frac{\sum_i c_i o_i}{\sum_i p_i o_i}$ is defined in Eq (2). We can then normalize x into $[0, 1]$ through min-max normalization for simplification. E can be used to indicate whether trajectory τ break the CPC constraint. We can also design $\boldsymbol{y}(\tau)$ to include $E = 1$ to make the model generate bids that do not break the CPC constraint. Sometimes it is also important to adjust the bidding parameters given real-time feedback provided by the advertiser to enable flexibility. Here we use two example indicators that reflect the experience of advertisers:

(1) **Smoothness**: an advertiser may expect the cost curve as smooth as possible to avoid sudden change. By defining $x = \frac{1}{T}\sum_t |cost_t - cost_{t-1}|$, we can model it as a binary variable S indicating whether the max cost change between adjacent time period exceeds a threshold as in Eq (14).
(2) **Early/Late Spend**: an advertiser may expect the budget to be cost in the morning or in the evening when there are promotions. Here we model the ratio of cost in the early half day through $x = \frac{\sum_{t=0}^{T/2} cost_t}{\sum_{t=0}^{T} cost_t}$, and use a binary variable to indicate whether the spend in the early half day exceeds a certain threshold C as in Eq (14).

We can also compose several constraints together to form $\boldsymbol{y}(\tau)$ to guide the model to generate bid parameters that adhere to different constraints. In this setting, $\boldsymbol{y}(\tau)$ will be a vector.

4.4 Complexity Analysis

The complexity analysis for training DiffBid consists of the training process and the inference process. For training, given the time complexity of the noise prediction model ϵ_θ is $O(T_1)$, the complexity for the inverse dynamic model f_ϕ is $O(T_2)$, the complexity for a training epoch is $O(|\mathcal{B}|(T_1 + T_2))$. It can be seen that the training complexity is linear with the input given T_1 and T_2 are relatively fixed. Thus the training of DiffBid is efficient. For generation, given the total diffusion step K, the trajectory length L, then the time complexity for inference is $O(KL(T_1+T_2))$. We can observe that the time complexity for inference is linearly scaled with the diffusion step K. In image generation, K is usually very large to ensure good generation quality, which brings the problem of non-efficiency. However, for bidding generation, we find K needs not to be very large. Relatively small K has already generated promising results. Moreover, in auto-bidding, a higher tolerance for latency is acceptable, enabling the use of relatively larger K.

5 THEORETICAL ANALYSIS

In this section, we theoretically analyze the property of DiffBid. In specific, we show that DiffBid that utilize MLE as the objective has a corresponding non-Markovian decision problem [16, 33, 36, 41]. The detailed proofs can be found in the Appendix A.7.

Lemma 5.1 (MLE as non-Markovian decision-making). *Assuming the Markovian transition $p_{y^*}(s_{t+1}|s_t, a_t)$ is known, the ground-truth conditional state distribution $p^*(s_{t+1}|s_{0:t})$ for demonstration sequences is accessible, we can construct a non-Markovian sequential decision-making problem, based on a reward function $r_\alpha(s_{t+1}, s_{0:t}) := \log \int p_\alpha(a_t|s_{0:t}) p_{y^*}(s_{t+1}|s_t, a_t) da_t$ for an arbitrary energy-based policy $p_\alpha(a_t|s_{0:t})$. Its objective is*

$$\sum_{t=0}^{T} \mathbb{E}_{p^*(s_{0:t})}\left[V^{p_\alpha}(s_{0:t})\right] = \mathbb{E}_{p^*(s_{0:T})}\left[\sum_{t=0}^{T}\sum_{k=t}^{T} r_\alpha(s_{k+1}; s_{0:k})\right] \tag{15}$$

$V^{p_\alpha}(s_{0:t}) := \mathbb{E}_{p^*(s_{t+1:T}|s_{0:t})}\left[\sum_{k=1}^{T} r_\alpha(s_{t+1}; s_{0:t})\right]$ is the value function of p_α. This objective yields the save optimal policy as the Maximum Likelihood Estimation $\mathbb{E}_{p^*(s_{0:T})}\left[\log p_\theta(s_{0:T})\right]$.

Remarks. This analysis shows that DiffBid utilizing MLE objective has its corresponding non-Markovian decision problem, and their optimal are equivalent. It means that DiffBid does not require the MDP assumption of problems and thus is more powerful in handling randomness and sparse return like in the advertising environment.

6 EXPERIMENTS

6.1 Experimental Setup

6.1.1 ***Experimental Environment***. The simulated experimental environment is conducted in a manually built offline real advertising system (RAS) as in [35]. Specifically, the RAS is composed of two consecutive stages, where the auction mechanisms resemble those in the RAS. We consider the bidding process in a day, where the episode is divided into 96 time steps. Thus, the duration between any two adjacent time steps t and $t + 1$ is 15 minutes. The number of impression opportunities between time step t and $t + 1$ fluctuates from 100 to 500. Detailed parameters in the RAS are shown in Table 5. We keep the parameters the same for all experiments.

6.1.2 ***Data Collection***. We use the widely applied auto-bidding RL method USCB in the online environment to generate the bidding logs for offline RL training. This results in a total 5,000 trajectories for the based dataset and 50,000 for a larger one. To increase the

4.3 条件设计。

本节介绍将工业界指标转化为 DiffBid 条件的方法。

4.3.1 基于回报的生成。对于每条轨迹 τ，我们将广告主获得的总价值作为回报 $R(\tau) = \sum_{t=1}^{T} r_t$。我们通过下式对回报进行归一化：

$$R = \frac{R(\tau) - R_{\min}}{R_{\max} - R_{\min}}, \tag{13}$$

其中， $R_{\min}$和 $R_{\max}$分别是数据集中的最小回报和最大回报。通过式13，我们将回报归一化为 $[0, 1]$，并将其合并到 $y(\tau)$中。随后，我们训练模型，使其以归一化后的回报为条件生成轨迹。需要注意的是，获得价值越多的轨迹，其归一化回报越高。因此， $R = 1$表示价值最高的最佳轨迹，它将更好地满足广告主的需求。在生成阶段，我们只需设置 $R = 1$，并在最大回报条件下为广告主生成轨迹。

4.3.2 基于约束或人类反馈的生成。在 MCB 中，应控制一个给定回合内与约束相关的累积表现，使其不超出广告主的预期。在这种设定下，我们可以设计 $\boldsymbol{y}(\tau)$来控制生成过程。例如，在 Target-CPC 设定下，我们可以维护一个二元变量 E，以表示最终的单次点击成本是否超过给定约束 C：

$$E = \mathrm{I}_{x \le C}(x) \tag{14}$$

其中， $x = \frac{\sum_i c_i o_i}{\sum_i p_i o_i}$在式（2）中定义。为简化起见，我们随后可以通过最小—最大归一化将 x归一化为$[0, 1]$。 E可用于表示轨迹 τ是否违反 CPC 约束。我们还可以设计 $\boldsymbol{y}(\tau)$，使其包含 $E = 1$，从而让模型生成不违反 CPC 约束的出价。有时，根据广告主提供的实时反馈调整出价参数以实现灵活性也很重要。这里，我们使用两个反映广告主体验的示例指标：

⑴ 平滑性：广告主可能希望成本曲线尽可能平滑，以避免突变。通过定义 $x = \frac{1}{T}\sum_t |cost_t - cost_{t-1}|$，我们可以将其建模为二元变量$S$，表示相邻时间段之间的最大成本变化是否超过某个阈值，如式（14）所示。

⑵ 早／晚花费：广告主可能希望在早上或晚上的促销期间花费预算。在这里，我们通过 $x = \frac{\sum_{t=0}^{T/2} cost_t}{\sum_{t=0}^{T} cost_t}$对前半天的成本占比进行建模，并使用一个二元变量表示前半天的花费是否超过某个阈值 C，如式（14）所示。

我们还可以将多个约束组合成 $\boldsymbol{y}(\tau)$，以引导模型生成符合不同约束的出价参数。在这种设定下， $\boldsymbol{y}(\tau)$将是一个向量。

4.4 复杂度分析

DiffBid 的复杂度分析包括训练过程和推理过程。对于训练，给定噪声预测模型 ϵ_θ的时间复杂度为 $O(T_1)$，逆动力学模型 f_ϕ的复杂度为 $O(T_2)$，则一个训练轮次的复杂度为 $O(|\mathcal{B}|(T_1 + T_2))$。可以看出，当 T_1和 T_2相对固定时，训练复杂度与输入呈线性关系。因此，DiffBid 的训练是高效的。对于生成，给定总扩散步数 K和轨迹长度 L，推理的时间复杂度为 $O(KL(T_1+T_2))$。我们可以观察到，推理的时间复杂度随扩散步数 K线性增长。在图像生成中， K通常非常大，以确保良好的生成质量，这会带来效率低下的问题。然而，对于出价生成，我们发现 K不必非常大。相对较小的 K就已产生了很有潜力的结果。此外，在自动出价中，可以接受更高的延迟容忍度，因此能够使用相对较大的 K。

5 理论分析

本节从理论上分析 DiffBid 的性质。具体而言，我们表明，以最大似然估计（MLE）为目标的 DiffBid 存在一个与之对应的非马尔可夫决策问题 [16, 33, 36, 41]。详细证明见附录 A.7。

引理 5.1（将 MLE 视为非马尔可夫决策）。假设已知马尔可夫状态转移$p_{y^*}(s_{t+1}|s_t, a_t)$，且可获取示范序列的真实条件状态分布 $p^*(s_{t+1}|s_{0:t})$，则我们可以基于奖励函数 $r_\alpha(s_{t+1}, s_{0:t}) := \log \int p_\alpha(a_t|s_{0:t}) p_{y^*}(s_{t+1}|s_t, a_t) da_t$，为任意基于能量的策略 $p_\alpha(a_t|s_{0:t})$构建一个非马尔可夫序贯决策问题。其目标为

$$\sum_{t=0}^{T} \mathbb{E}_{p^*(s_{0:t})}\left[V^{p_\alpha}(s_{0:t})\right] = \mathbb{E}_{p^*(s_{0:T})}\left[\sum_{t=0}^{T}\sum_{k=t}^{T} r_\alpha(s_{k+1}; s_{0:k})\right] \tag{15}$$

$V^{p_\alpha}(s_{0:t}) := \mathbb{E}_{p^*(s_{t+1:T}|s_{0:t})}\left[\sum_{k=1}^{T} r_\alpha(s_{t+1};\ s_{0:t})\right]$是 p_α的价值函数。这一目标产生的最优策略与最大似然估计 $\mathbb{E}_{p^*(s_{0:T})}\left[\log p_\theta(s_{0:T})\right]$相同。

说明。这一分析表明，采用 MLE 目标的 DiffBid 存在与之对应的非马尔可夫决策问题，且二者的最优解等价。这意味着 DiffBid 不要求问题满足 MDP 假设，因此在处理广告环境这类场景中的随机性和稀疏回报时更具能力。

6 实验

6.1 实验设置

6.1.1 实验环境。仿真实验在人工构建的离线真实广告系统（RAS）中进行，与 [35] 相同。具体而言，RAS 由两个连续阶段组成。其拍卖机制与真实广告系统中的机制相似。我们考虑一天内的出价过程，将该回合划分为 96 个时间步。因此，任意两个相邻时间步 t和 $t + 1$之间的时长为 15 分钟。时间步 t与 $t + 1$之间的曝光机会数量在 100 到 500 之间波动。RAS 的详细参数见表 5。所有实验均使用相同的参数。

6.1.2 数据收集。我们在在线环境中使用广泛应用的自动出价 RL 方法 USCB，生成用于离线 RL 训练的出价日志。由此，基础数据集共获得5,000条轨迹，更大的数据集共获得50,000条轨迹。为增加

Figure 14. AIGB, source page 5: final bilingual output used as a development training sample. Dense inline notation, display equations, a theorem, and numbered behavioral constraints stress object preservation and reading order. This version includes the corrected two-item list, bold labels, and hanging indentation.

Table 2: Ablation Study

Model	USCBEx-5K	USCBEx-50K
DiffBid	2280.12	2395.60
DiffBid w/o cond	1812.64	1852.21
DiffBid w/o non-mkv	2254.78	2287.41

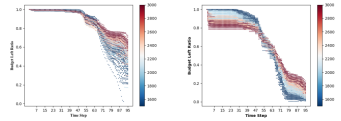
from the results is the impact of training dataset size on model performance. When comparing the "USCB-5K" and "USCBEx-50K" settings, it becomes evident that a larger training dataset consistently leads to improved cumulative rewards. This finding underscores the significance of data size in training RL models for automated bidding. A richer dataset allows the models to capture more diverse bidding scenarios and make more informed decisions, ultimately resulting in better performance. One intriguing aspect of DiffBid's performance is its resilience to noise. In real-world advertising environments, there can be inherent uncertainty and variability in the bidding process due to factors like market dynamics and competitor behavior. DiffBid appears to handle such noise more effectively than the RL baselines. This means that even in situations where bidding outcomes are less predictable, DiffBid manages to maintain competitive performance.

6.3 Ablation Study

To study different parts of the proposed DiffBid, we run the model without a certain module to see if the removed corresponding module will result in a performance drop. The result of the ablation study is shown in Table 2. Due to the space limitation, we only provide the results on USCBEx-5K and USCBEx-50K. w/o cond refers to the DiffBid with the condition set to 0.0 (rather than 1.0). w/o non-mkv refers to the situation where we only use the current state and the predicted next state to generate the bidding coefficient. From the table, we find both of the two parts contribute to the final result, and removing either of them will result in a performance drop. It verifies the effectiveness of the proposed methods in boosting DiffBid's performance for auto-bidding.

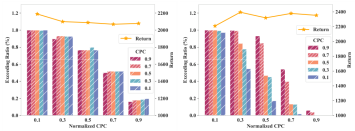
6.4 In-depth Analysis

6.4.1 ***Study of State Transition.*** Here we compare the state transition of the baseline method USCB and our proposed method DiffBid. The result for grouped and non-grouped state transition during a day is shown in Figure 3. In this figure, we plot the budget left ratio with time steps in one day. From the figure, we can observe that under USCB, most of the advertisers' consumption does not exhaust their budget. This is attributed to the inconsistency between the offline virtual environment and the real online environment faced by USCB. On the contrary, the budget completion situation improves under DiffBid, where most of the advertisers spend more than 80% of their budgets. One possible reason is that DiffBid finds trajectories with a high budget completion ratio will also have a high cumulative reward, and thus tend to generate trajectories with a high budget completion ratio. Moreover, advertisers with small budgets undertend to spend money in the afternoon. This is because the impressions in the afternoon offer a higher cost-effectiveness, albeit with a limited quantity.



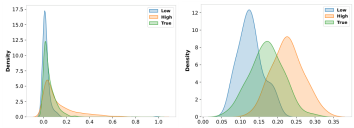
(a) USCB (b) DiffBid

Figure 3: State Transition in One Episode.



(a) IQL (b) DiffBid

Figure 4: Performance under CPC constraint.



(a) Smoothness (b) Early Spend

Figure 5: Performance of Human Feedback.

6.4.2 ***Performance under Constraints and Feedbacks.*** We additionally investigate DiffBid's multi-objective optimization capability under specific constraints, comparing its performance with Offline RL. Specifically, we choose CPC ratio and overall return as metrics and examine the ability of DiffBid and IQL to control the overall CPC exceeding ratio while maximizing the overall return. During training, we set different thresholds of CPC as in Eq (14). Then when testing, we make DiffBid generating trajectories under the expected CPC. In Figure 4, we show the exceeding ratio and overall return under different CPC constraints and training settings. From the figure, we find that DiffBid has the ability to control diverse levels of exceeding ratio while maintaining an intact return, surpassing IQL by a significant margin. Consequently, DiffBid holds a distinct advantage in effectively addressing MCB problems. We also study the performance under different advertiser

Table 2: Ablation Study

Model	USCBEx-5K	USCBEx-50K
DiffBid	2280.12	2395.60
DiffBid w/o cond	1812.64	1852.21
DiffBid w/o non-mkv	2254.78	2287.41

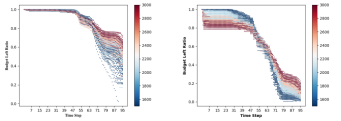
这些结果还反映出训练数据集规模对模型性能的影响。比较"USCB-5K"和"USCBEx-50K"设定时，可以明显看出，更大的训练数据集始终带来更高的累积奖励。这一发现凸显了数据规模对训练自动出价强化学习模型的重要性。更丰富的数据集使模型能够捕捉更多样的出价情境，并做出依据更充分的决策，最终取得更好的性能。DiffBid 性能中一个值得关注的方面是其抗噪能力。在真实广告环境中，由于市场动态和竞争对手行为等因素，出价过程可能存在固有的不确定性和变化。DiffBid 似乎比强化学习基线更能有效应对此类噪声。这意味着，即便在出价结果较难预测的情况下，DiffBid 仍能保持具有竞争力的性能。

6.3 消融研究

为研究所提出的 DiffBid 的各个部分，我们在移除某个模块的情况下运行模型，以观察移除相应模块是否会导致性能下降。消融研究结果如表2所示。由于篇幅限制，我们仅提供 USCBEx-5K 和 USCBEx-50K 上的结果。w/o cond 表示将条件设为 0.0（而非 1.0）的 DiffBid。w/o non-mkv 表示仅使用当前状态和预测的下一状态来生成出价系数的情况。从表中可以看出，这两个部分均对最终结果有所贡献，移除其中任何一个都会导致性能下降。这验证了所提出的方法能够有效提升 DiffBid 在自动出价中的性能。

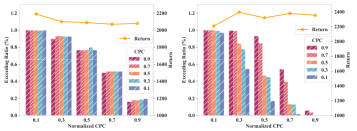
6.4 深入分析

6.4.1 状态转移研究。这里，我们比较基线方法 USCB 与所提出的 DiffBid 方法的状态转移。一天内分组和未分组的状态转移结果见图 3。图中绘制了一天内剩余预算比例随时间步的变化。由图可见，在 USCB 下，大多数广告主的消费没有用尽预算。这是由于 USCB 所面对的离线虚拟环境与真实在线环境存在不一致。相比之下，DiffBid 下的预算完成情况有所改善，大多数广告主花费了 80% 以上的预算。一种可能的原因是，DiffBid 发现预算完成率高的轨迹也具有较高的累积奖励，因此倾向于生成预算完成率较高的轨迹。此外，预算较少的广告主倾向于在下午花费预算。这是因为下午的曝光机会性价比更高，但数量有限。



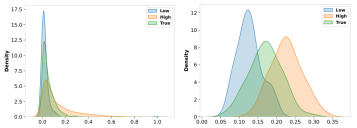
(a) USCB (b) DiffBid

图 3：一个回合内的状态转移。



(a) IQL (b) DiffBid

图 4：CPC 约束下的表现。



(a)平滑性 (b)提前支出

图 5：人类反馈的表现。

6.4.2 约束和反馈下的表现。我们还研究了 DiffBid 在特定约束下的多目标优化能力，并将其表现与离线 RL 进行比较。具体而言，我们选择 CPC 比率和总体回报作为指标，考察 DiffBid 和 IQL 在最大化总体回报的同时控制总体 CPC 超出比例的能力。在训练期间，我们按照式（14）设置不同的 CPC 阈值。随后，在测试时，让 DiffBid 在期望的 CPC 条件下生成轨迹。图 4 展示了不同 CPC 约束和训练设置下的超出比例及总体回报。由图可见，DiffBid 能够在保持回报不受损失的同时控制不同水平的超出比例，显著优于 IQL。因此，DiffBid 在有效解决 MCB 问题方面具有明显优势。我们还研究了不同广告主

Figure 15. AIGB, source page 7: final bilingual output used as a development training sample. An ablation table and three groups of plots share a two-column page with explanatory prose. The final output preserves the table and plot content while maintaining readable captions and subplot labels.

at any time t, has the partial information $\mathbf{x}_t$ fully available and can progressively estimate:

$$\mathbf{x}_0 \approx \hat{\mathbf{x}}_0 = \left(\mathbf{x}_t - \sqrt{1-\bar{\alpha}_t}\boldsymbol{\epsilon}_\theta(\mathbf{x}_t)\right)/\sqrt{\bar{\alpha}_t} \tag{15}$$

due to Eq. (4). (A stochastic reconstruction $\mathbf{x}_0 \sim p_\theta(\mathbf{x}_0|\mathbf{x}_t)$ is also valid, but we do not consider it here because it makes distortion more difficult to evaluate.) Figure 5 shows the resulting rate-distortion plot on the CIFAR10 test set. At each time t, the distortion is calculated as the root mean squared error $\sqrt{\|\mathbf{x}_0 - \hat{\mathbf{x}}_0\|^2/D}$, and the rate is calculated as the cumulative number of bits received so far at time t. The distortion decreases steeply in the low-rate region of the rate-distortion plot, indicating that the majority of the bits are indeed allocated to imperceptible distortions.

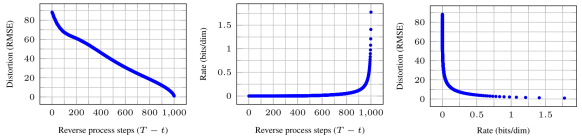


Figure 5: Unconditional CIFAR10 test set rate-distortion vs. time. Distortion is measured in root mean squared error on a $[0, 255]$ scale. See Table 4 for details.

Progressive generation We also run a progressive unconditional generation process given by progressive decompression from random bits. In other words, we predict the result of the reverse process, $\hat{\mathbf{x}}_0$, while sampling from the reverse process using Algorithm 2. Figures 6 and 10 show the resulting sample quality of $\hat{\mathbf{x}}_0$ over the course of the reverse process. Large scale image features appear first and details appear last. Figure 7 shows stochastic predictions $\mathbf{x}_0 \sim p_\theta(\mathbf{x}_0|\mathbf{x}_t)$ with $\mathbf{x}_t$ frozen for various t. When t is small, all but fine details are preserved, and when t is large, only large scale features are preserved. Perhaps these are hints of conceptual compression [18].



Figure 6: Unconditional CIFAR10 progressive generation ($\hat{\mathbf{x}}_0$ over time, from left to right). Extended samples and sample quality metrics over time in the appendix (Figs. 10 and 14).



Figure 7: When conditioned on the same latent, CelebA-HQ 256 × 256 samples share high-level attributes. Bottom-right quadrants are $\mathbf{x}_t$, and other quadrants are samples from $p_\theta(\mathbf{x}_0|\mathbf{x}_t)$.

Connection to autoregressive decoding Note that the variational bound (5) can be rewritten as:

$$L = D_{\mathrm{KL}}(q(\mathbf{x}_T) \,\|\, p(\mathbf{x}_T)) + \mathbb{E}_q\left[\sum_{t\geq 1} D_{\mathrm{KL}}(q(\mathbf{x}_{t-1}|\mathbf{x}_t) \,\|\, p_\theta(\mathbf{x}_{t-1}|\mathbf{x}_t))\right] + H(\mathbf{x}_0) \tag{16}$$

(See Appendix A for a derivation.) Now consider setting the diffusion process length T to the dimensionality of the data, defining the forward process so that $q(\mathbf{x}_t|\mathbf{x}_0)$ places all probability mass on $\mathbf{x}_0$ with the first t coordinates masked out (i.e. $q(\mathbf{x}_t|\mathbf{x}_{t-1})$ masks out the t^{th} coordinate), setting $p(\mathbf{x}_T)$ to place all mass on a blank image, and, for the sake of argument, taking $p_\theta(\mathbf{x}_{t-1}|\mathbf{x}_t)$ to

在任意时刻 t，都已完整获得部分信息 $\mathbf{x}_t$，并据此逐步估计：

$$\mathbf{x}_0 \approx \hat{\mathbf{x}}_0 = \left(\mathbf{x}_t - \sqrt{1-\bar{\alpha}_t}\boldsymbol{\epsilon}_\theta(\mathbf{x}_t)\right)/\sqrt{\bar{\alpha}_t} \tag{15}$$

这是由于式（4）。（随机重建 $\mathbf{x}_0 \sim p_\theta(\mathbf{x}_0|\mathbf{x}_t)$同样有效，但本文不予讨论，因为这会使失真评估更加困难。）图 5展示了在 CIFAR10 测试集上得到的率失真曲线。在每个时刻 t，失真按均方根误差$\sqrt{\|\mathbf{x}_0 - \hat{\mathbf{x}}_0\|^2/D}$计算，码率则按截至时刻 t已接收比特的累计数量计算。率失真曲线在低码率区域的失真急剧下降，这表明大多数比特确实都用于编码不可感知的失真。

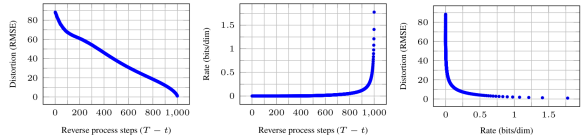


图 5：无条件 CIFAR10 测试集的率失真随时间变化曲线。失真以 $[0, 255]$ 尺度上的均方根误差衡量。详情见表 4。

渐进式生成 我们还通过从随机比特开始进行渐进式解压缩，运行了一个无条件渐进生成过程。换言之，我们在使用算法 2 对反向过程采样时，预测反向过程的结果 $\hat{\mathbf{x}}_0$。图 6和 10展示了反向过程进行期间 $\hat{\mathbf{x}}_0$ 的样本质量。大尺度图像特征最先出现，细节则最后出现。图 7展示了随机预测 $\mathbf{x}_0 \sim p_\theta(\mathbf{x}_0|\mathbf{x}_t)$在 $\mathbf{x}_t$固定时针对不同 t的结果。当 t较小时，除细微细节外的内容都得以保留；当 t较大时，只保留大尺度特征。这或许为概念压缩提供了一些线索[18]。



图 6：无条件 CIFAR10 渐进式生成（$\hat{\mathbf{x}}_0$ 随时间变化，从左至右）。附录中给出了扩展样本以及样本质量指标随时间的变化（图 10和 14）。



图 7：在相同潜变量条件下，CelebA-HQ 256 × 256生成的样本具有相似的高层属性。右下象限为 $\mathbf{x}_t$，其余象限为从 $p_\theta(\mathbf{x}_0|\mathbf{x}_t)$采样得到的样本。

与自回归解码的联系 注意，变分界（5）可以改写为：

$$L = D_{\mathrm{KL}}(q(\mathbf{x}_T) \,\|\, p(\mathbf{x}_T)) + \mathbb{E}_q\left[\sum_{t\geq 1} D_{\mathrm{KL}}(q(\mathbf{x}_{t-1}|\mathbf{x}_t) \,\|\, p_\theta(\mathbf{x}_{t-1}|\mathbf{x}_t))\right] + H(\mathbf{x}_0) \tag{16}$$

（推导见附录 A。）现在考虑将扩散过程的长度 T设为数据的维数，并定义前向过程，使得 $q(\mathbf{x}_t|\mathbf{x}_0)$将全部概率质量集中在 $\mathbf{x}_0$ 上，同时屏蔽前 t个坐标（即 $q(\mathbf{x}_t|\mathbf{x}_{t-1})$屏蔽第 t个坐标）；令$p(\mathbf{x}_T)$将全部概率质量置于一张空白图像上；再姑且设 $p_\theta(\mathbf{x}_{t-1}|\mathbf{x}_t)$为

Figure 16. DDPM, source page 7: final bilingual output used as a development training sample. Rate–distortion plots and generated-image grids are interleaved with captions and mathematical expressions. The final output includes repaired native hats, bold variables, and subscripts in prose and captions.